Fall 12-20-2017

Femtosecond Laser Micromachining of Low-Temperature Co-Fired Ceramic and Glass Fiber Reinforced Polymer Printed Circuit Boards Materials

Raif Farkouh
University of Nebraska - Lincoln, raiffarkouh91@gmail.com

Femtosecond Laser Micromachining of Low-Temperature Co-Fired Ceramic and Glass Fiber Reinforced Polymer Printed Circuit Boards Materials

By

Raif Farkouh

A THESIS

Presented to the Faculty of

The Graduate College at the University of Nebraska

In Partial Fulfillment of Requirements

For the Degree of Master of Science

Major: Electrical Engineering

Under the Supervision of Professors Yongfeng Lu and Ambrose Wolf

Lincoln, Nebraska

December 2017

Femtosecond Laser Micromachining of Low-Temperature Co-Fired Ceramic and Glass Fiber Reinforced Polymer Printed Circuit Boards Materials

Raif Farkouh, M.S.

University of Nebraska, 2017

Advisors: Yongfeng Lu and Ambrose Wolf

Low-temperature co-fired ceramic (LTCC), and glass fiber reinforced polymer (GFRP) printed circuit boards (PCBs) are two materials used for the packaging of electronics. The excellent mechanical and electrical properties of LTCC, combined with the ability to embed passive components offer superior radio frequency (RF) performance and device miniaturization for high-frequency applications. Due to its unique properties, LTCC provides superior performance in applications as diverse as military radar, imaging systems, advanced automotive sensing, telecommunications, and satellites. The use of LTCC in these applications has created a demand for the micromachining of holes, channels, and cavities with specific geometries and structures. Likewise, GFRP PCBs are the backbone of the electronics industry. They work to mechanically support and electrically connect components using conductive tracks, pads and other features etched from copper sheets laminated onto GFRP substrate. Since the electronics industry has been moving toward devices with smaller size and lower cost, there has been an increasing need to drill holes in GFRP PCBs with high quality and efficiency.

Some of the conventional techniques used to machine LTCC and GFRP PCBs are micro punching, mechanical milling, and electrical discharge machining. These

techniques can machine some structures on LTCC and GFRP PCBs, but the drawbacks such as geometry-limitation, wear and tear of tools, high-cost, complex equipment, lack of flexibility and crack-tendency limit the application of these techniques. Femtosecond laser micromachining is a comparatively new technique that offers a solution to meet the challenging demand for drilling of LTCC and GFRP PCBs. The unique properties of ultrashort pulse width and the extremely high peak intensity allow fs laser to drill high-quality holes and to minimize thermal and mechanical damage by the term of "cold" ablation mechanism.

In this project, efficient processes for femtosecond laser drilling of LTCC and GFRP PCBs for RF packaging were developed. A high drilling quality with no trace of dross, debris and reacting layer was achieved. The effects of the laser parameters, including pulse energy, scanning speed, focal position, and pitch, on the hole quality, were investigated. A laser polishing process of LTCC was also developed since the reduction of surface roughness is of practical importance for achieving low microwave loss.

ACKNOWLEDGEMENT

I would like to express my sincere gratitude to my advisors Drs. Yongfeng Lu and Ambrose Wolf for the continuous support throughout my Master's program, for their patience, motivation, enthusiasm, and immense knowledge. Their guidance on both research as well as on my career has been invaluable. I gratefully appreciate the financial support received from the DOE's Kansas City National Security Campus (KCNSC), managed by Honeywell under contract number DE-NA0002839. My deep appreciation goes out to Dr. Ambrose Wolf and Sean Garrison for their invaluable advice and feedback on my research, and leadership for the Radar 2021 Consortium. I also express my thanks to Dr. Lisha Fan, Dr. Zhe Lin, and everyone working in the LANE Lab for not only being willing to help me work through problems and answer questions, but for making my time in the lab fun and enjoyable. Special thanks to Dr. Ianno, Dr. Yang and Dr. Han for being on my graduate committee. Finally, I would like to thank my mom, dad, and brother for teaching me the importance of a good education, and always being there to encourage me.

TABLE OF CONTENTS

LIST OF FIGURES

LIST OF ABBREVIATIONS

FE-SEM: Field-emission Scanning Electron Microscopy.

FEG: Field Emission Gun.

LaB_6: Lanthanum Hexaboride.

W: Tungsten.

CSI: Coherence Scanning Interferometry.

CCD: Charge-coupled Device.

RMS: Root Mean Square.

ns: Nanosecond.

fs: Femtosecond.

HAZ: Heat Affected Zone.

LTCC: Low-Temperature Co-Fired Ceramics.

PCBs: Printed Circuit Boards.

GFRP: Glass Fiber Reinforced Polymer.

RF: Radio Frequency.

CNC: Computer Numerical Control.

2D: Two-dimensional.

3D: Three-dimensional.

N_2: Nitrogen.

$\emptyset_0$: The Original Laser Fluence.

$\emptyset_{eff}$: The Effective Laser Fluence.

EDM: Electrical Discharge Machining.

CHAPTER 1: INTRODUCTION

1.1 Research Motivations

1.2 Thesis Outline

1.1 Research Motivations

A Laser “light amplification by simulated emission of radiation” is a device that emits light through a process of optical amplification based on simulated emission of electromagnetic radiation. [1] A Laser emits a coherent and amplified beam of electromagnetic radiation that can propagate in a straight line. The rapid development of lasers with a wavelength ranging from the ultraviolet to the infrared range, pulse duration from nanosecond (ns) to femtosecond (fs) has led to wide-range applications. Laser material processing has evolved since 1960 and revolutionized many industries by providing innovative solutions in numerous industrial engineering applications, including welding, heat treatment, laser forming, shock peening, micromachining, and nano-processing. [2] High-intensity short or ultrashort laser pulses are a powerful energy source for creating features in diverse materials by precise ablating with little or no collateral damages. [3] Laser material processing has several advantages over conventional material processing techniques: 1. As a non-contact thermal process, it eliminates problems associated with mechanical processing, such as contamination of the workpiece; 2. The operation cost is low due to avoidance of tool wear; 3. The heat effect on the surrounding areas minimized during laser processing attributed to the short interaction time and high intensity. [4]

One of the growing laser applications is laser drilling. The advantages of using lasers against conventional methods for drilling include the ability of drilling holes with high quality and precision, and reduced processing time to meet industry growing requirements and standards. Holes with dimensions in the order of microns with high aspect ratios (depth-to-diameter ratio much higher than 10) can be drilled using lasers.

Laser drilling has been employed in applications such as jet engine turbine airfoils, aerospace turbine-engine cooling holes, automotive, and medical industries. [5] Laser processing quality highly depends on laser parameters (wavelength, pulse duration, fluence, repetition rate, etc.), material properties (thickness, shape, chemical composition, hardness, and physical properties.). Thermal distortion creates a heat affected zone (HAZ) near the drilling zone if the temperature rises above the critical transformation point, leading to issues such as wall damage, micro-cracks, and debris. Laser drilling creates more stresses in material than other conventional methods such as waterjet cutting. [6]

The primary goal of this research is to develop efficient processes for fs laser drilling of low-temperature co-fired ceramic (LTCC) and printed circuit boards (PCBs) for radio frequency (RF) electronic packaging. High drilling quality with no trace of dross, debris and reacts layer was achieved. Another process developed in this research work is laser polishing of LTCC.

This project aims to further advance laser processing of LTCC and PCBs for RF electronics packaging applications and extends the understanding of the processes. It is intended to develop a process capable of achieving high-quality drilling by studying different types of lasers, laser parameters and processing strategies for quality improvement.

The objectives of this research are summarized as follows:

- To investigate the fundamental characteristics of fs laser micromachining of LTCC and GFRP PCBs.
- To investigate the effects of laser parameters on the laser drilling quality.

- To demonstrate the capability of fs laser drilling of LTCC and GFRP PCBs.
- To develop a high quality (HAZ-free, crack-free) fs laser drilling processes for LTCC and GFRP PCBs.
- To demonstrate the capability of polishing LTCC using different types of lasers including continues-wave and pulsed lasers.

1.2 Thesis Outline

The most significant contributions of this dissertation carried out at Laser-Assisted Nano Engineering (LANE) lab – UNL are: 1) Developing a process for fs laser drilling of LTCC, 2) Developing a process for laser polishing of LTCC, and 3) Developing a process for fs laser drilling of PCBs.

This dissertation includes six chapters. In chapter 1, the motivations of this study are detailed, and the dissertation outline provided. In chapter 2, laser processing fundamentals and its capabilities reviewed. Advantages of laser material processing described. The fundamental laser drilling mechanisms are also reviewed, including laser-matter interaction, the critical process parameters, and characteristics of laser drilling. The critical parameters of laser drilling were elaborated so that the relevant principles underlying the process are identified. The experimental equipment employed in this research work including the laser systems and characterization equipment was described. In chapter 3, the experimental work carried out on fs laser drilling of LTCC and the influence of different laser parameters on the drilling quality characteristics was studied. High-quality drilling with no damage and free HAZ were achieved by optimizing the processing parameters. In chapter 4, fs laser drilling on PCBs with a gas assisted focusing

system was demonstrated, and the influence of different laser parameters on the drilling quality was investigated. In chapter 5, laser polishing of LTCC was demonstrated. The characteristics of laser interaction with the material were discussed. The influence of different laser systems on the polishing quality was investigated. The optimized polishing parameters were presented. Finally, a summary of this research work was provided, and recommendations for future research were discussed in chapter 6.

Chapter 2: Background and Reviews

2.1 Introduction

This chapter introduces laser systems and laser processing fundamentals. As the major topic of the thesis, laser drilling was discussed in a separate section because of the unique characteristics of the process. A detailed description of laser drilling mechanism was provided to understand the essential process characteristics and material removal mechanisms. Types of lasers used in laser machining were also introduced. The critical parameters and quality characteristics typically considered in laser drilling were discussed.

2.2 Laser Material Processing

The laser is a coherent and amplified beam of electromagnetic radiation that can propagate in a straight line. The key element in making a practical laser is the light amplification achieved by stimulated emission due to the incident photons of high energy. Laser light differs from ordinary light because it has photons of the same frequency, wavelength, and phase. [7] Thus, unlike regular light, the laser beam is highly directional with high power density and high focusing characteristics. The laser generates electromagnetic radiation with a wavelength ranging from the ultraviolet to the infrared range. [8] The power generated by the laser can be as low as 1 mW and as high as 100 KW. Laser power could be delivered to a focus position with a precise spot size/dimension and spatial/temporal distribution on a given substrate. [9] At the same time, the monochromatic, coherent, and low divergence properties of the laser enable them to produce high energy concentrations. When a laser beam is focused, it works as a

source of intense heat. As a result of its unique properties, the laser can be used to heat, melt, and vaporize materials for a wide range of applications. Industrial laser applications include deposition, welding, cutting, removal, and alteration of material property through changing its configuration. [10] The key parameters that affect processing quality include beam power, wavelength, beam form (continues or pulsed), beam distribution and beam quality. This chapter describes the principle of laser material processing and provides an overview of its engineering applications.

2.2.1 Advantages and Disadvantages of Laser Material Processing

Laser material processing has several advantages over conventional machining techniques. Meanwhile, lasers have a number of disadvantages that make them less suitable for specific applications. The advantages and disadvantages of laser processing are discussed below [8-10-11]:

Advantages:

- The high-intensity laser beam, as a highly localized heating source, minimizes the heat effect on the surrounding areas attributed to the ability to focus the beam to a small size. Meanwhile, it offers high geometry accuracy, and capability to achieve features as small as 1 micrometer with submicron tolerances.
- Due to the non-contact nature of the process, laser processing does not require clamping of the workpiece, avoiding the mechanical damage and contamination from the clamping. It also reduces operation costs by avoidance of tool wear.
- Ease of automation and control. The beam power can be easily manipulated by controlling the current through the electric discharge. At the same time, laser

machining processes are easy to automate with computer numerical control (CNC machining) and robotic processing, which provides high control over the dimensions and speeds of the process.

- Laser machining provides high accessibility using mirrors and fiber optic cables.
- Laser machining systems are highly flexible and can be configured to perform different processes (cutting, drilling, welding, and engraving).

Disadvantages:

- Relatively high capital investment. The capital cost needed to purchase a laser can be considerable.
- Low power efficiency, and energy waste while the laser is not in continuous use.
- The laser beam is harmful if it comes in contact with human workers. It can cause severe burns if it happens accidentally.

2.2.2 Laser Processing Applications

Laser processing has been used in the automobile, shipbuilding, aerospace, steel, electronics, and medical industries for precision machining of complex parts. [12] The main laser processing applications include: drilling, cutting, turning/ milling, welding, cladding, marking, surface treatment, and micromachining. Micromachining refers to machining of features having dimensions below 1 mm. Ultrashort pulse lasers (pulse duration varies from ns to fs) have been shown to be an attractive option for the high-quality micromachining of many materials due to their ability to minimize damage and precise processing. [13]

Laser drilling has become the accepted economical process for drilling thousands of closely spaced holes. Three types of laser drilling exist: single-pulse/multi-pulse percussion drilling and trepanning drilling. Trepan drilling involves cutting around the circumference of the hole to be generated, whereas percussion drilling 'punches' directly through the workpiece with no relative movement of the laser or workpiece. [10]

Laser cutting has found applications in punching, cutting and marking of metals, ceramics, and plastics. Laser cutting is superior to other conventional or non-conventional cutting techniques because of material versatility, no wear or change of tool, high material utilization, production flexibility, high accuracy, and edge quality. [14] Three types of laser cutting exist: fusion cutting, sublimation cutting, and photochemical ablation. Fusion cutting involves localized melting of the base material, which is then ejected using high-pressure assist gas. The assist gas could be oxygen, which reacts with the material and provides energy to support the process, or it could be an inert gas. In sublimation cutting, a pulsed beam is utilized to vaporize along the cutting seam of the workpiece. The vaporized material is ejected using an inert assist gas. In photochemical ablation, an ultraviolet laser beam is utilized to irradiate a very thin layer near the surface of an organic material. Since organic materials tend to absorb ultraviolet radiation efficiently, the molecular bonds break, leading to the material removal of the irradiated area. [15]

Laser turning and milling is a three-dimensional process that requires two lasers to get the desired profile in the workpiece. The beams are focused at desired angles with the help of fiber optics. Laser milling allows the production of parts with complex shapes without expensive tooling. Laser milling is most suitable for machining parts with one-

sided geometry or partial machining of components from one side only. Complete laser milling of parts is also possible but accurately re-positioning the work-part is a big challenge. [16]

Laser welding is advantageous over conventional welding processes in that it welds at faster speeds and higher weld strength. [17]

Laser cladding is used to coat weak parts with a harder material to improve the surface quality. Recently, laser cladding was used to produce ceramic-metal composite coatings that have low dilution, a dense microstructure, metallurgical bonding to the substrate, high wear resistance, and high corrosion resistance. [18]

2.2.3 Types of Laser Systems

To optimize laser processing for specific applications and materials, it is essential to select a suitable laser. The correct laser needs to be chosen to optimize the principal process parameters, which include the laser wavelength, beam power, beam distribution, beam form (continuous or pulsed), and the beam distribution.

Lasers consist of three principal parts: active medium to provide gain, an optical cavity to enhance and control the optical field, and a pumping source to provide the energy. The gain medium is a material with properties that allow it to amplify light with stimulated emission. Additional provisions for cooling the mirrors, guiding the beam, and manipulating the target are necessary to facilitate material processing. [19] The type of laser and its wavelength depend on the laser medium. The laser medium could be a solid (e.g. Nd: YAG), liquid (e.g. dye) or gas (e.g. CO_2, He/Ne). [20] There are different types of lasers used in material processing including carbon neodymium-doped yttrium

aluminum garnet (Nd: YAG) lasers, dioxide (CO_2) lasers, ultra-short pulse Ti: Sapphire lasers, ytterbium-doped fiber lasers, and excimer (KrF, ArF, XeCl) lasers. [21]

2.3 Laser Drilling

Laser drilling is the process of creating thru-holes by applying a focused laser beam to heat up the material to its melting point or vaporization temperature. Depending upon material thickness and properties, very small diameter holes can be achieved (of the order of microns) using laser drilling, which in return results in high aspect ratios. Laser drilling has become the accepted economical process for drilling thousands of closely spaced holes. Laser drilling has been used in such applications as jet engine turbine airfoils, aerospace turbine-engine cooling holes, automotive, and medical industries and sectors. [5] The main beam characteristics that influence laser drilling process are: wavelength, reputation rate (number of pulses per second), pulse duration, pulse energy, and beam quality.

2.3.1 Methods of Laser Drilling

Four types of laser beam drilling exist, as shown in Fig. 2.1:

1. Single-pulse (one center) drilling.
2. Percussion drilling.
3. Trepanning drilling.
4. Helical Drilling.

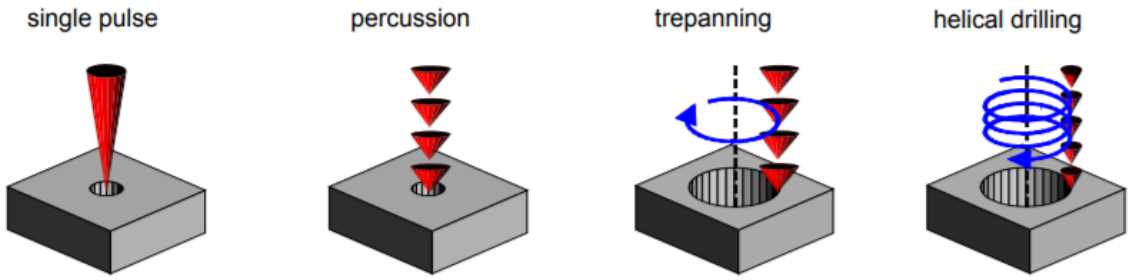

Figure 2.1: Schematic illustration of laser drilling strategies. [22]

Single-pulse drilling: The process involves applying a laser beam with a pulse duration of about 1 ms, and energy of several joules. At its focusing point, the beam results in peak power of the order of 100 KW. The material in contact with the laser beam absorbs the laser beam, partly melts, and partly evaporates. The melted and evaporated material is blown out of the hole using a gas assisted system. Single-pulse drilling requires very high pulse energy to drill deep holes by reducing the laser frequency with low productivity. Single-pulse drilling is best used for applications requiring holes with a small thickness. [23,24,25]

Percussion drilling: The process involves applying a series of laser pulses with low pulse energy and short pulse duration. Due to the low peak power required in the process, the amount of molten material and plasma produced is minimized, which in return results in improved hole quality and reduced wall taper. This allows percussion drilling to realize the desired drilling depth with thicker materials. The created holes are deeper, more precise, and have a smaller diameter than those obtained using single-pulse drilling. The evaporated material is ejected out of the hole by the excess pressure of the gas in the hole. [23,24,25]

Trepanning: Trepanning drilling is a combined drilling and cutting process that is capable of producing large diameter holes. It involves cutting around the circumference

of the hole to be generated. The laser beam travels over the hole area in increasingly larger circular tracks to ablate the whole surface area. The material produced is blown away downward. Larger diameter holes with improved quality can be obtained. [23,24,25]

Helical Drilling: Helical drilling is a drilling technique that breaks up the process into a multitude of ablation steps to enhance the accuracy. In contrast to trepanning, the helical drilling reaches the breakthrough only after many turns of spiral describing the path of the ablation front. Helical drilling has the following favorable effects on drilling accuracy: more deviation from circular geometry can be reduced than trepanning; the load on the opposite walls is minimized; and most importantly, recast layers as observed in percussion drilling can be greatly reduced or completely avoided. The beam path is not limited to circular geometry. With suitable optical systems like scanners or by movement of the workpiece, any shape can be formed. [24,25]

2.3.2 Laser Drilling Process Parameters

The properties of the processed material and the required quality and geometry of the drilled holes are the two main factors which determine the type of laser selected for a given drilling application. The main laser drilling parameters are:

1. Beam parameters.
2. Drilling characteristics.
3. Process defects.

Beam parameters:

The main beam parameters that influence laser drilling process are: (a) frequency (number of pulses per second). (b) Pulse energy: Generally, hole depth increases as increasing the pulse energy. At the same time, high pulse energy leads to deformation at the entrance surface of the hole, and therefore reducing the quality. (c) Pulse duration: The hole quality generally improves with shorter beam pulses, while the number of pulses required to drill a hole increases too. (d) Beam quality: Higher quality beam enhances the hole quality for small diameter holes due to its small diameter and long focus depth, allowing longer penetrating depth. [23]

Drilling characteristics:

The main characteristics of laser drilling are: (a) hole diameter: Holes with a diameter in the range of μm to mm can be achieved using laser drilling. It could be challenging to maintain the depth of focus to create holes with a diameter smaller than 2 μm. (b) Drilling angle: It is the angle between the beam axis and the workpiece. The beam power density is maximized at a drilling angle of 90^{o}. (c) hole depth.

Process defects:

The quality of the drilled hole is affected by the HAZ, taper, and microcracks. Thermal distortion creates a HAZ if the temperature rises above the critical transformation point, resulting in microcracks (see Fig. 2.2).

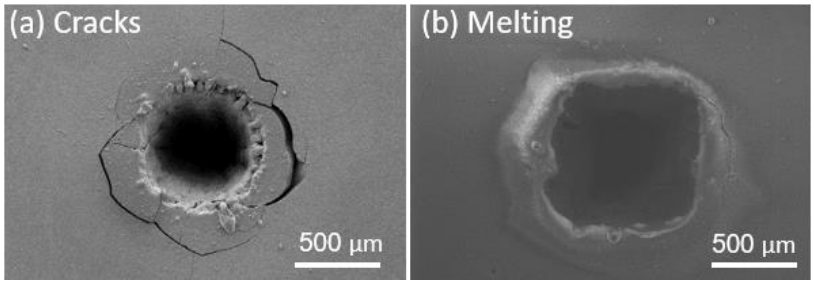

Figure 2.2: SEM images of laser processing defects due to HAZ: (a) cracks, and (b) melting.

Heat affected zone in laser drilling is localized near the drilling zone. Erosion of molten and vaporized material from the hole and the conical shape of the laser beam result in the tapering of the drilled hole (see Fig. 2.3). The taper degree depends on the pulse energy and pulse duration. Taper decreases when the effective focal length of the laser decreases. Tapering is a critical issue for deep hole drilling, while it can be ignored for very small hole depths. Another common defect in laser drilling is recast, which is caused by the remaining of the re-solidified excess molten and vaporized material that is not entirely removed.

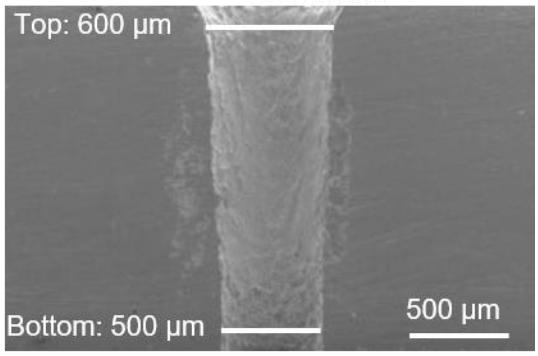

Figure 2.3: SEM cross-sectional image of a tapered hole.

2.4 Mechanisms of Laser Ablation

Laser ablation is a process of precise material removal by irradiating with a laser beam. The ablation of materials occurs above specific threshold fluence. The magnitude of threshold fluence depends on laser beam parameters such as pulse duration, energy, and wavelength, along with the target material properties, microstructure, surface morphology and the presence of defects. [26] With long laser pulses, much of the pulse energy contributes only to heating the sample surface, and the heat spreads into the surrounding area and contributes to the formation of a HAZ. With a short pulse duration, a higher proportion of the pulse energy is delivered above the threshold power level, maximizing processing while minimizing the HAZ (see Fig. 2.4).

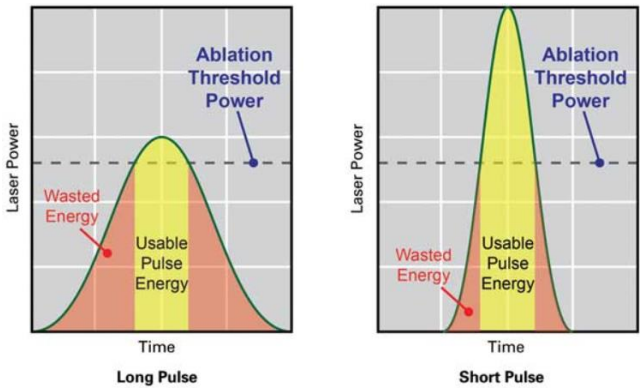

Figure 2.4: The effects of pulse duration on laser ablation. [27]

When multiple pulses are used for laser ablation, the ablation thresholds decrease due to incubation effect. [28] Femtosecond laser ablation has an important advantage compared with ablation using longer pulses because it removes material with little or no collateral damage. [29]

Laser Ablation with Femtosecond Laser:

The main advantage of fs laser ablation comes from the timescales involved in material interactions with the fs pulses. For fs lasers, electrons are excited up to a few to tens of electron volts in tens of femtoseconds, while energy transfer from electrons to ions occurs in the order of picoseconds. Therefore, the laser energy is absorbed by the electrons, leaving the ions cold, and thermalization takes place after the laser pulse is gone. This leads to significant reduction in thermal damage, and HAZ. [30]

Femtosecond laser energy is absorbed by electrons during the pulse irradiation. The two primary ionization mechanisms are: 1) multiphoton ionization and 2) avalanche ionization. A fs laser can achieve very high intensities (typically > 10^{13} W/cm^2), at which seed free electrons are generated by multiphoton ionization. Multiphoton ionization occurs because of the high photon flux of fs laser, which leads to several photons of energy below the ionization threshold "simultaneously" striking a bound electron. When the total energy of the absorbed photons is higher than the ionization threshold, the bound electron is freed from the valence band. On the other hand, impact ionization occurs when an electron with sufficient kinetic energy obtained by absorbing photons, transfer part of its energy to a bounded electron by collisions to overcome the ionization potential and produce two free electrons. Consequently, the free electrons absorb photons and generate more free electrons from the bound electrons. Such a series of impacts is called avalanche ionization, where free electron density exponentially increases. Avalanche ionization strongly depends on free electron density. [31] The dissipation of the absorbed energy in bulk material, and the corresponding material removal takes place mostly after the laser pulse duration.

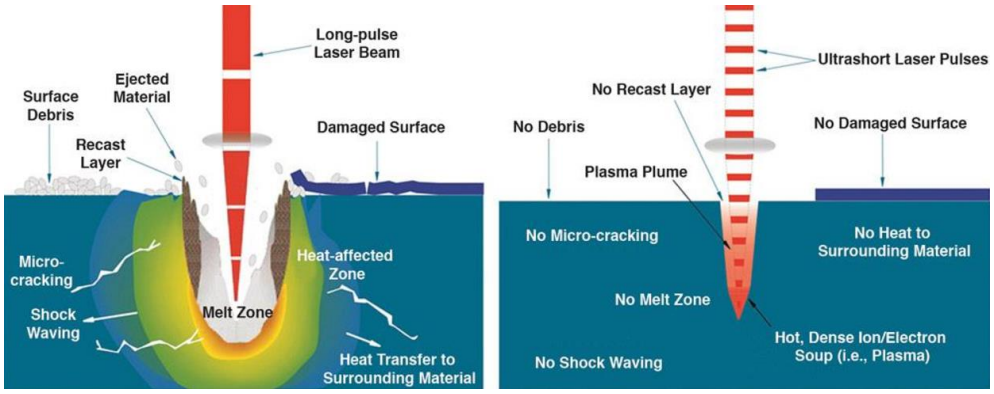

Figure 2.5: (Right) Long laser pulses deliver a high amount of heat that spread throughout the workpiece causing micro-cracking and melting. (left) Ultrafast lasers remove material by a cold process, eliminating cracking and HAZ (right). [32]

The two major mechanisms of fs material removal are: 1) thermal vaporization, where the electron-phonon collisions increase the local temperature above the vaporization point, and 2) Coulomb explosion, where excited electrons are ejected from the target surface and form a strong electric field, the resultant electric field pulls out the ions out of the target, which results in removing several nanometers of the lattice within the skin depth. [33] According to these two mechanisms of material removal, fs laser ablation can be divided into two regimes: strong ablation dominated by thermal vaporization at intensities significantly higher than the ablation threshold, and gentle ablation governed by the Coulomb explosion at intensities near the ablation threshold. [34]

2.5 Experimental Apparatus and Analytical Equipment

The samples were subject to several characterization methods. Field-emission scanning electron microscope (FE-SEM), laser scanning microscope, and three-dimensional (3D) optical profiler were used to evaluate the morphology and quality of the machined structures. The following paragraphs provide a brief description of the characterization techniques employed throughout this study. The physical principles and the major elements constituting the equipment are detailed.

2.5.1 Field-Emission Scanning Electron Microscopy (FE-SEM)

One benefit of using an FE-SEM to analyze surface features is the ability to obtain a high magnification and high-resolution image that provides a two-dimensional (2D) image of the 3D structures. An FE-SEM is a microscope that works with electrons. Electrons are generated by a field emission source. The sample is placed in a high vacuum chamber, allowing electron movement along the column without scattering and preventing discharges inside the gun zone. Afterwards, the sample is scanned with a beam of accelerated electrons to image its surface. Emitter type is the main difference between the SEM and the FESEM. Traditional SEM systems use thermionically emitted electrons generated from a heated tungsten (W) or lanthanum hexaboride (LaB_6) filament; while an FE-SEM uses field emission gun (FEG) as a source of electrons. A field emission gun is a wire of W fashioned into a sharp Field emitting tip, the tip is held at a very high potential to an electrode. The potential is so large that the electrons are released from the tip of the emitter. [35] Once the electrons are released, they are sent

through electromagnetic lenses, which use varying magnetic fields to deflect and focus the charged particles. After focusing, the beam goes through a series of deflector plates, which are used to scan the beam over the surface of the sample. The electron beam interacts with the sample and produces secondary electrons, which are picked up and interpreted by a detector. [36] In this research, we used a Hitachi 4700 FE-SEM system (see Fig. 2.7). The Hitachi 4700 FE-SEM system has a magnification range: 20 up to 500,000× magnification and 1.2 nm resolution. The samples are bombarded with electrons accelerated at a high voltage under a vacuum of 10^{-9} torr.

Figure 2.6: Hitachi 4700 FE-SEM system.

2.5.2 Keyence Laser Scanning Microscope VK-X200K

The laser scanning microscope used for this work was a Keyence VK-X200K laser scanning microscope (see Fig. 2.8). The VK-X200K laser scanning microscope is a confocal laser scanning microscope. It provides non-contact, nanometer-level profile, roughness, and film thickness data on any materials without the need for sample preparation. Keyence VK-X200K laser scanning microscope builds a 3D composition of a surface and measure parameters from the composition. One key feature of a confocal

microscope is that a pinhole is placed in front of the photoreceptor. The optics are tuned such that light from the focal point of the beam interacting with the sample can pass through the pinhole. This means only a slice of the 3D structures imaged by the sample can be in focus at once and the remaining light is blocked out. Two-dimensional images are taken point-by-point by moving the sample vertically and changing the level at which the sample is observed. The VK-X200K is capable of creating 3-D images with 0.5 nm resolution steps between each 2D slice. [37]

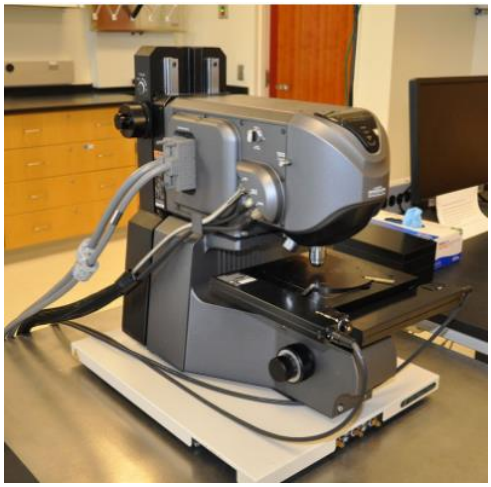

Figure 2.7: VK-X200K laser scanning microscope.

2.5.3 Zygo NewView 8300 3-D Optical Profiling System

The surface roughness and structure height were determined using a Zygo NewView 8300 3D Optical Profiling System (see Fig. 2.9), a white light interferometer system. It offers fast, non-contact, high-precision 3D metrology of surface features. It includes proprietary data analysis and system control software Mx™ software. The profiler uses Coherence Scanning Interferometry (CSI). The system is capable of measuring a wide range of surface types, including smooth, rough, flat, sloped, and stepped. The profile heights with a range from < 1 nm up to 20000 µm, at high speeds,

independent of surface texture, magnification, or feature height. It offers surface topography repeatability of 0.12 nm.

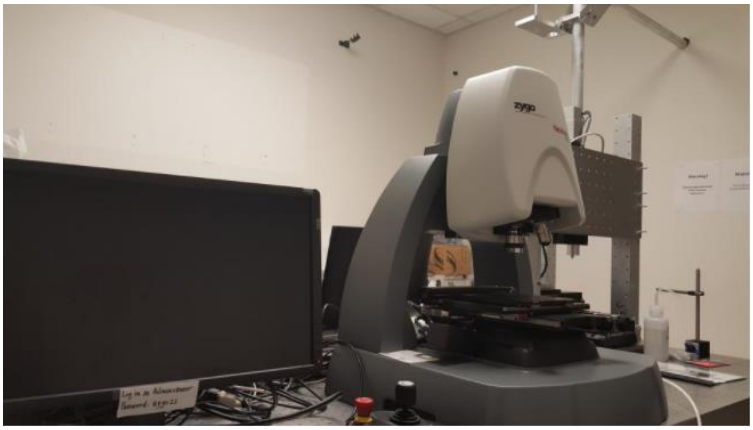

Figure 2.8: Zygo NewView 8300 3-D Optical Profiling System.

Chapter 3: Femtosecond Laser Drilling of Low-Temperature Co-Fired Ceramic

---

3.1 Introduction

Low-temperature co-fired ceramic is difficult to machine due to its brittle failure and crack on finished surfaces. Low-temperature co-fired ceramic has been machined using various advanced machining processes such as micro punching, mechanical milling and electrical discharge machining (EDM). [38] The above methods are limited due to disadvantages, such as low material removal rate, expensive tool, high tool wear, time-consuming, and low surface finish. Femtosecond laser processing offers unique advantages, such as high-precision material processing, thereby providing the potential for efficient drilling of deep holes with reduced recast/microcracks, and no HAZ.

In this work, femtosecond laser drilling of LTCC was demonstrated, and two fs laser systems were employed for LTCC drilling in ambient air: a fs Ti: Sapphire laser and a fiber fs laser system. The effects of the laser parameters, including pulse energy, scanning speed, focal position, and pitch, on drilling quality, were investigated. The shape and morphology of the holes were characterized and evaluated using laser microscope and SEM. The hole taper and the HAZ were evaluated. The influence of the experimentally controllable parameters on the measured outputs was analyzed and discussed. Debris-free holes with good roundness, straight and clean trench edges and no thermal damage were achieved.

3.2 Material Properties

Low-temperature co-fired ceramic stands for a ceramic substrate system, which constituent materials are metal and ceramic. The ceramic is co-fired with metal wiring at low temperature. Its low sintering temperature (approximately 900°C) allows co-firing with highly conductive metals such as silver and gold. Printed gold and silver conductors or alloys with platinum or palladium are used in general.

The excellent mechanical and electrical properties of LTCC substrates, combined with the ability to embed passive components and to apply fine line patterning, offer superior RF performance and device miniaturization for high-frequency applications. Further features like the application of heat sinks, frames and nail head pins by brazing allow for hermetic and highly complex packages. Due to its unique properties, LTCC materials provide superior performance in applications as diverse as military radar, imaging systems, advanced automotive sensing, telecommunications, and satellites. [39]

3.3 Ti: Sapphire Femtosecond Laser Drilling of LTCC

3.3.1 Experimental Setup

Figure 3.1 shows the schematic of the fs laser drilling setup. The drilling source was a Ti: Sapphire fs laser system equipped with an amplifier (Legend F, Coherent Inc., 150 fs, 1 kHz, 800 nm). An attenuator was used to tune the incident laser energy. The laser beam was focused to a spot of 10 μm in diameter using a 20× objective lens. The output collimated beam is a nearly symmetric Gaussian with $M_2 < 1.3$, and a maximum output pulse energy of 1 mJ. Samples were placed on a linear motion XYZ stage. The stage has a travel range of 100 mm in the X-Y direction and 50 mm in the Z direction.

The maximum moving speed of the stage is 5000 mm/s with an accuracy of ± 2 µm. The linear motion stage was controlled by computer software. A mechanical shutter has been used to switch the laser beam. A charge-coupled device (CCD) camera was placed along the optical axis and used to align the sample and obtain a live view of the laser processing. The process was performed in open air without any sample pre-treatment.

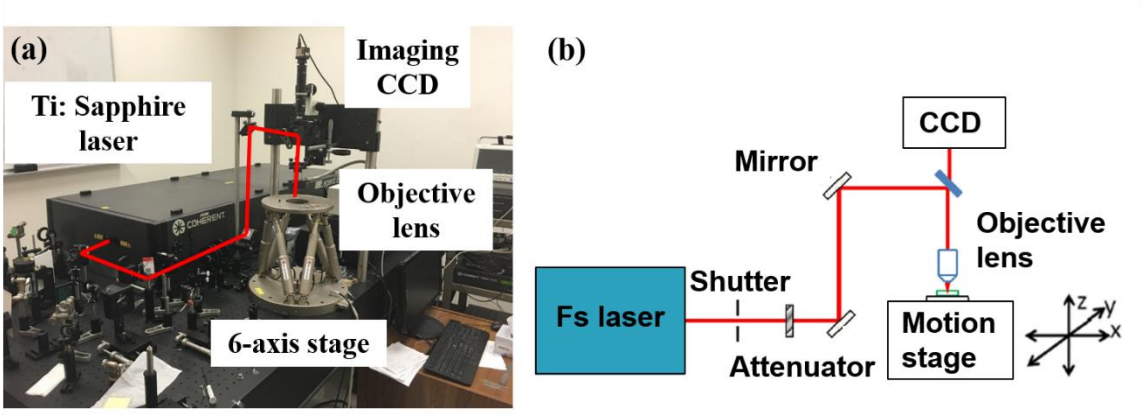

Figure 3.1: (a) A photo, and (b) a schematic illustration of the Ti: Sapphire laser drilling experiment setup.

3.3.2 Drilling Strategy

In this study, helical drilling was used since it can generate large holes with good consistency and taper. Helical drilling was realized by using the linear translational stage with a plano-convex lens with a focal length of 100 mm. A number of passes were required for the complete drilling of the LTCC material. Figure 3.2 shows the path of laser scanning. The laser beam was vertically focused on the LTCC surface that was fixed in position. The LTCC sample was placed on the XYZ linear motion stage. The sample was guided using a horizontal rectangular wave scanning motion. The scanning line resulted in a rectangular cavity with a depth equal to the focal depth of the lens. Afterward, the sample was moved upward with a suitable pitch to reposition the laser

focal position on the top surface of the sample. Again, the sample was guided using a vertical rectangular wave scanning motion. The sequence was repeated until a through hole was obtained. All experiments were performed in ambient air and without shielding gas. The linear motion stage was controlled by a computer.

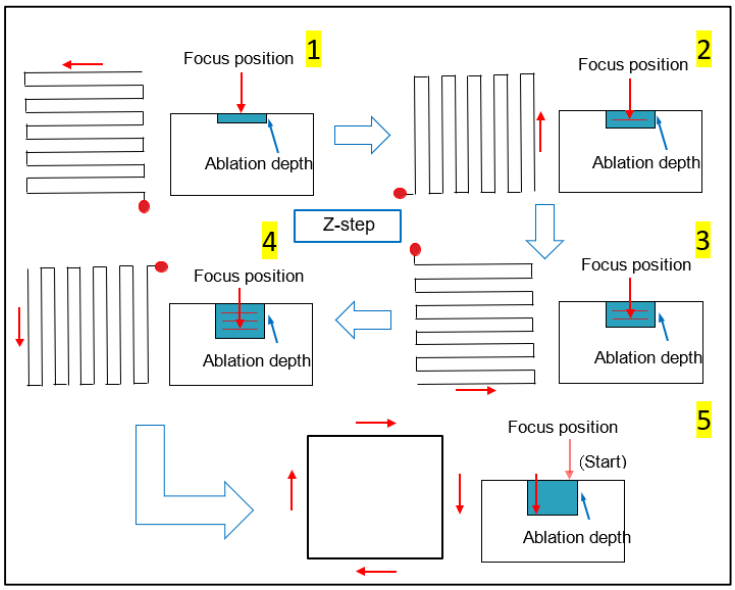

Figure 3.2: Illustration of the laser scanning path.

3.3.3 Results and Discussion

In order to optimize the drilling process, the effects of the laser parameters, including pulse energy, scanning speed, focal position, and pitch, on the drilling quality were investigated. The repetition rate, wavelength, and pulse duration were fixed and set to 1 kHz, 800 nm, and 150 fs, respectively. Rectangular holes were drilled in LTCC with a thickness of 1.6 mm.

3.3.3.1 Process Defects and Problems Solved

The quality of the drilled hole was affected by the HAZ, taper, and microcracks (see Fig. 3.3). The crack formation was caused by too much heat accumulation because the heat had no time to dissipate when the hole was drilled on a thick LTCC substrate. Heat accumulation created a HAZ near the drilling area when the temperature rose above the critical transformation point, resulting in microcracks and wall damage (see Fig. 3.3 (c)). Debris was observed on the entrance side (see Fig. 3.3 (b)). Debris formed when the material volume was removed from the hole during the drilling process. Since it is completely perforated, melt and vapor were driven out through the entrance side, which led to the contamination of entrance side. As shown in Figs. 3.3 (d) and (e), the surface at the entrance side was significantly contaminated with melt and condensed vapor. In particular, the edges were covered with debris (see Fig. 3.3 (b)).

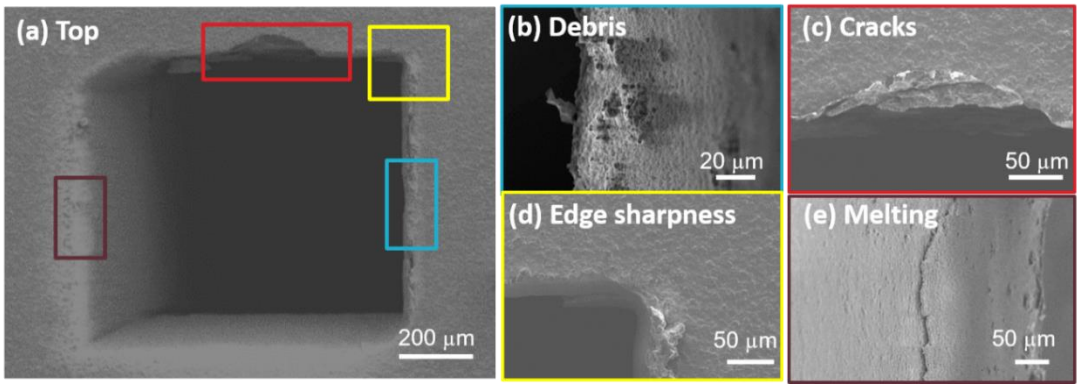

Figure 3.3: SEM detailed images of the drilling defects: (a) top view, (b) sidewall debris, (c) cracks, (d) edge sharpness, and (e) melting.

3.3.3.2 Taper

In laser helical drilling, a series of identical laser pulses were delivered to the drilling point until the hole was drilled through. As a diverging laser beam (after a focal point) propagated through the hole, wall absorption took place, and the laser power

density reduced as the hole depth increased, which in return resulted in the formation of a tapered hole. Also, the focused laser beam had a cone shape that produced a taper on the cut edges of the material. A process was investigated to reduce the hole taper.

The taper was defined by Eq. (1) (Fig. 3.4).

$$\text{Taper } (^\circ) = \frac{D-d}{2t} \times \frac{180^\circ}{\pi} \quad (1)$$

where *D* is the hole entrance diameter, *d* is the hole exit diameter, and *t* is the material thickness.

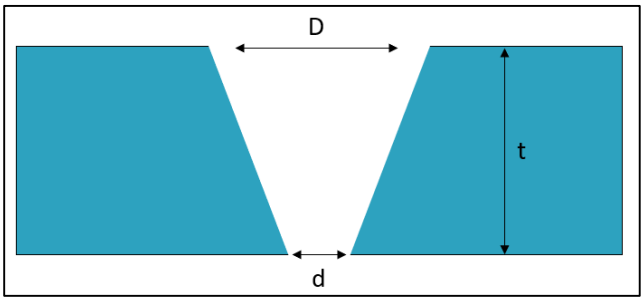

Figure 3.4: Schematic illustration of a hole profile and taper dimensions.

3.3.3.3 Effects of Laser Pulse Energy

The ablation depth using different laser pulse energies was investigated. A single-line ablation test was performed, and the depth of the ablated material was plotted as a function of the laser pulse energy in Fig. 3.5. The test was performed with a fixed scanning speed of 200 µm/s and a focal position on top of the surface.

The results show that the ablation rate increased linearly with the laser pulse energy. The maximum depth that was drilled with a single laser scan with a pulse energy of 500 µJ was 70 µm. In order to maximize the drilling process efficiency, laser pulse energy of 500 µJ was used to drill the PCBs material. High laser intensities are required to rapidly drill a through-hole with fs pulses. The laser beam has a Gaussian distribution with the energy in the spot center is highest, and the energy in the spot edge is low. After

a through-hole was drilled, the high-intensity part of the laser pulse propagates directly through the hole without absorption. The laser energy was close to the ablation threshold at the edge of the laser spot. Therefore, soft ablation occurred at the laser spot edge with only a small amount of material removed. Since only a small layer of material was removed from the walls, soft ablation was equivalent to a "polishing effect," remarkably improving the wall quality.

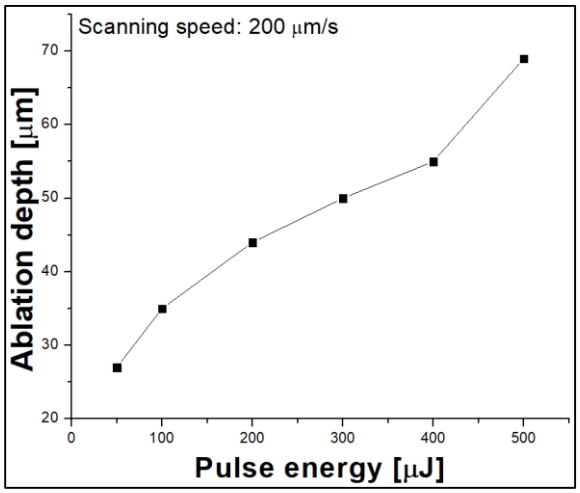

Figure 3.5: Ablation depth plotted as a function of laser pulse energy at a fixed scanning speed of 200 μm/s.

3.3.3.4 Effects of Focal position

Focus position determines the beam spot size and the laser power density on the sample surface. Laser power density plays a key role in the formation of the HAZ, wall quality, and drilling efficiency. The optimization process for the focus position was thus conducted at a laser pulse energy of 500 μJ, scanning speed of 1 mm/s, and a pitch of 50 μm. Holes were drilled with different focal positions. Figure 3.6 describes the focal position relative to the workpiece surface. A negative focal position stands for a focal

position above the workpiece surface. A positive focal position stands for a focal position below the workpiece surface.

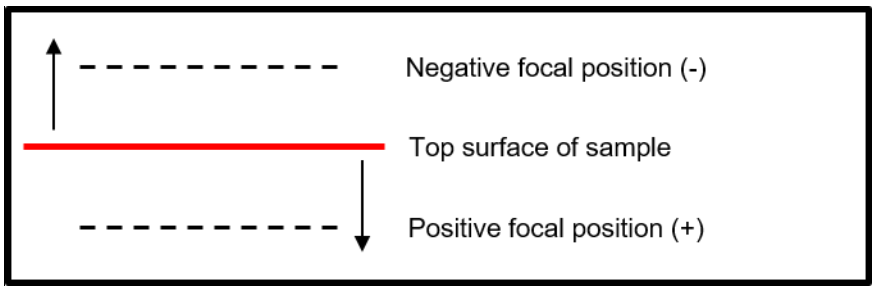

Figure 3.6: Illustration of the focal position relative to the workpiece surface.

For holes drilled with focal positions of +500 µm and -500 µm, obvious processing defects, including wall damage and debris were observed (see Fig. 3.7). This could be attributed to the fact that with focal positions of +500 µm and -500 µm, the laser was out of focus, which led to incomplete material removal due to insufficient laser power. For holes drilled with focal positions of 0 and -100 µm, better sidewall quality was observed (see Fig. 3.7).

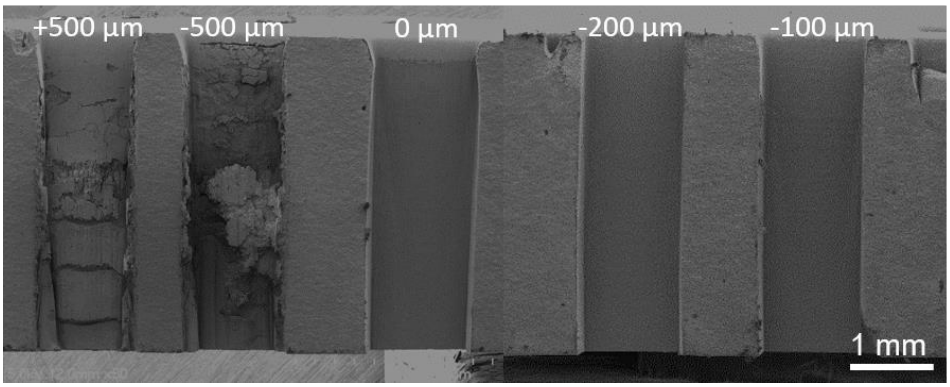

Figure 3.7: SEM cross-sectional image of holes drilled with different focal positions relative to the workpiece surface.

The optimized sidewall quality was obtained with a focal position 200 µm above the workpiece surface. At a -200 µm focal position, the Gaussian beam achieved larger

kerf width, allowing more material to be removed during the drilling process, which increased the final drilling quality. An SEM cross-sectional image of a hole drilled at a focal position 200 µm above the workpiece surface with laser pulse energy of 500 µJ, a scanning speed of 1 mm/s, and a pitch of 50 µm is shown in Fig. 3.8. Clean walls with no HAZ and no taper with sharp edges were achieved.

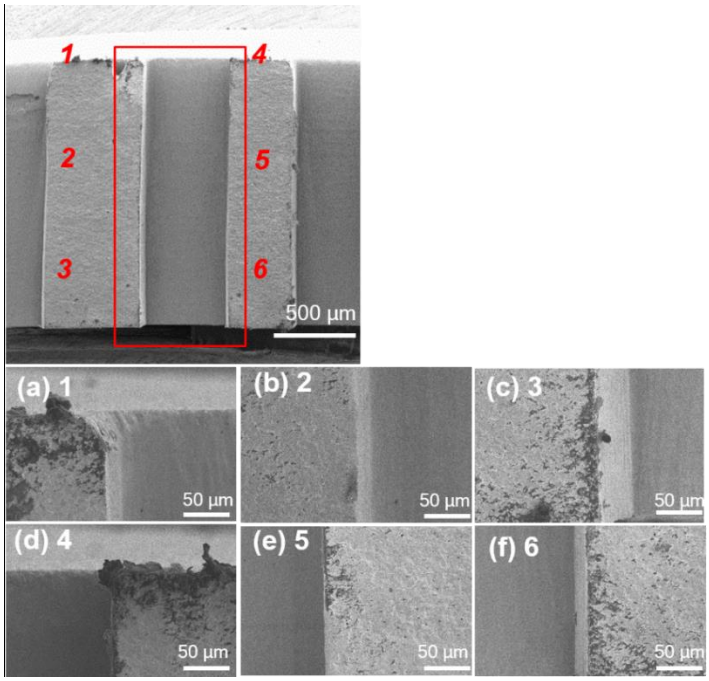

Figure 3.8: SEM cross-sectional image of a hole drilled with a focal position 200 µm above workpiece surface and high magnification images of different locations of the hole.

3.3.3.5 Effects of Pitch

The location of the tightly-focused laser spot, where the laser power density is highest, was strategically and precisely moved to keep the drilling process consistent for each hole from top to bottom and from hole to hole. We found that the optimal starting location at a focal position of 200 µm above the work surface. Maintaining the location of the laser focal spot relative to the workpiece has been a challenge since there has not been a way to measure it dynamically. To maintain a fixed distance of the laser focal spot

relative to the workpiece during the drilling process, the focal position started above the surface and moved down to the bottom surface step-by-step by “Pitch.” The focal position was moved after each drilling loop, where “n” is the total drilling loops (see Fig 3.9).

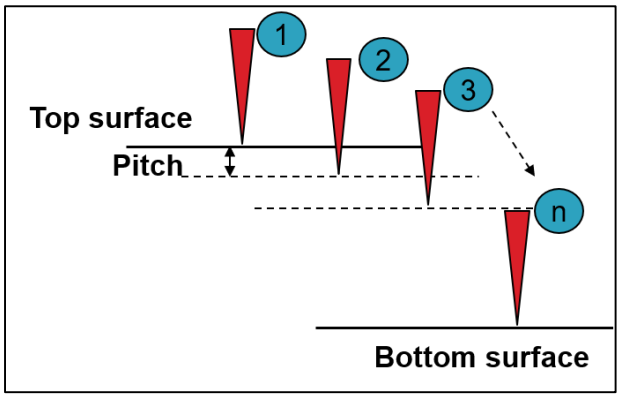

Figure 3.9: Schematic illustration of the movement of the laser focus position during the drilling process.

To find the optimal pitch for the drilling process, rectangular holes were drilled at different pitches. The drilling was conducted with pitch steps of 50, 100, and 500 µm at a laser pulse energy of 500 µJ, a scanning speed of 1 mm/s, and a focal position of 200 µm above the sample surface. Pitch affects the sidewall quality. If the pitch was too large (100 µm and above), the rate of ablation depth was slower than the movement of laser focal point, leading to a closed end hole (see Fig. 3.10 (c) and 3.10 (d)). Meanwhile, the insufficient laser power led to the formation of dross due to incomplete material removal. The smaller the pitch, the higher the sidewall quality is. The optimal pitch was found to be 50 µm (see Fig. 3.10 (b)).

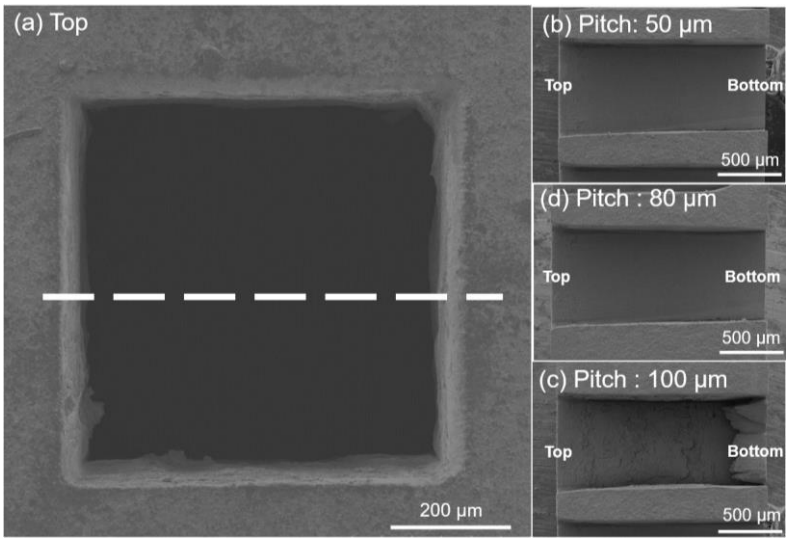

Figure 3.10: (a) SEM top image of a hole drilled at a pitch of 50 µm, and SEM cross-sectional images of holes drilled at different pitches: (b) 50, (c) 80, and (d) 100 µm.

3.3.3.6 Effects of Laser Scanning Speed

To investigate the effects of scanning speed on the drilling quality, rectangular holes were drilled with different scanning speeds. The drilling was conducted at scanning speeds from 1 to 2.5 mm/s for different round numbers until the substrate was drilled through. The laser pulse energy was set at 500 µJ with a focal position of 200 µm above the sample top surface and a pitch of 50 µm. Figure 3.11 shows the hole drilled with different scanning speeds. The higher the scanning speed is, the more efficient the drilling is. Drilling at a higher speed of 1.5 mm/s took less time to drill through the substrate, whereas drilling at a slower speed of 1 mm/s took a longer time to drill through the substrate. However, it was also found that drilling at higher scanning speeds reduces the drilling quality in terms of sidewall quality and taper (see Figs. 3.11 (c) and (d)). At higher drilling velocities of 1.5 and 2 mm/s, there existed some cracks and debris on the sidewall associated with significant large hole taper (see Fig. 3.11 (d) and (e)). Also, with a scanning speed of 2.5 mm/s, the bottom side of the hole was not completely removed

(see Fig. 3.11 (e)). Whereas at slower drilling speed of 1 mm/s, no cracks were observed, and the hole taper was reduced. This could be attributed to the fact that the scanning speed determines the pulse number deposited in one laser spot area. At a low scanning speed, more pulses were delivered to a single spot and more laser pulses overlapped during scanning of the laser beam. This resulted in higher energy delivered to one spot, and higher ablation rate. While at high scanning speed, the ablation rate was lower, and the bottom side of the hole was not completely removed (see Figs. 3.11 (e)).

Based on the above results, the optimal scanning speed was 1 mm/s. With a scanning speed of 1 mm/s, the drilling time of a hole in a 1.6 mm thick LTCC substrate took 37 minutes.

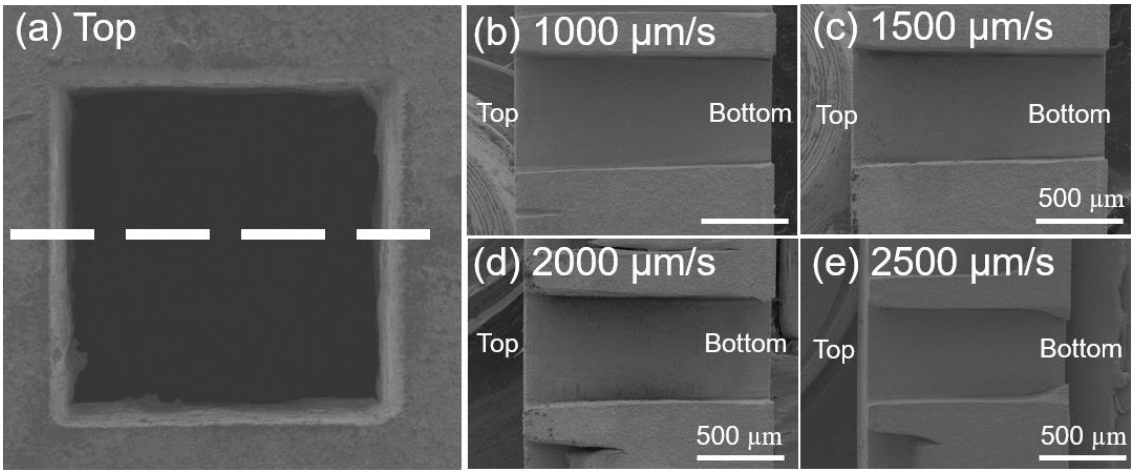

Figure 3.11: (a) SEM top image of a hole drilled at scanning speed of 1 mm/s, and SEM cross-sectional images of holes drilled at different scanning speeds: (b) 1000, (c) 1500, (d) 2000, and (e) 2500 µm/s.

3.3.3.7 Optimized Results

In Fig. 3.12, SEM images of the top and bottom sides of a hole drilled in a 1.6 mm thick LTCC substrate in the open air are shown. The hole was drilled using the optimized parameters: a laser pulse energy of 500 µJ, a focal position of 200 µm above

the sample top surface, a pitch of 50 µm, and a scanning speed of 1 mm/s. A difference in width between the top and bottom sides of the hole resulted from a slight taper. The taper was calculated to be 3º (see Fig. 3.12 (b)).

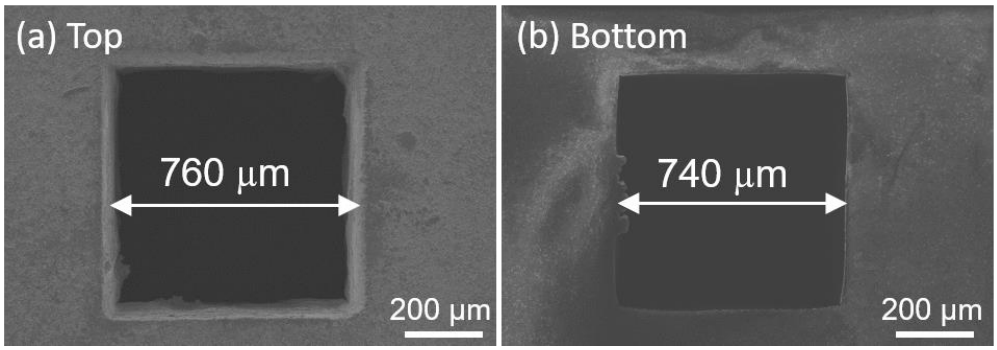

Figure 3.12: SEM images of a hole fabricated in a 1.6 mm-thick LTCC plate using optimized parameters: (a) top view, and (b) a bottom view.

As shown in Fig. 3.13, high-quality drilling with no visible microcracks in a 760 µm square hole was achieved. A cross-sectional image of the hole shows minimal sidewall taper and clean overall appearance (see Fig. 3.13 (d)). Issues of taper angle (Fig. 3.13 (b)), edge quality (Fig. 3.13 (e)), crack formation, and sidewall quality (Fig. 3.13 (c)) were all solved with optimal drilling parameters.

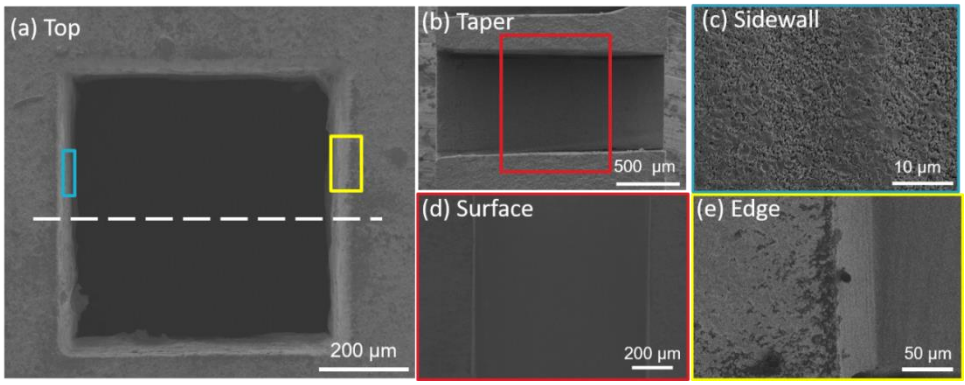

Figure 3.13: (a) SEM top image of a hole drilled using optimized parameters, and high magnification SEM images of different locations of the hole showing (b) taper, (c) sidewall, (d) surface, and (e) edge.

3.4 Fiber Femtosecond Laser Drilling of LTCC

3.4.1 Experimental Setup

The experimental setup used in this study is shown in Fig. 3.14. A near-infrared (NIR) fs laser (PolarOnyx Laser, Inc., Uranus 3200-1030-0800-PM, a central wavelength of 1030 nm, a pulse duration of 800 fs, pulse energy of 150 μJ, and repetition rate of 150 kHz) was used as the irradiation source. The laser beam was focused onto a target at an incident angle of 90°. The focal spot diameter was about 10 μm. The output collimated beam was a nearly symmetric Gaussian. A 2D galvanometer scanner was used to focus and scan the laser beam on the sample. The galvanometer scanner has a working range of 50×50 mm and a focal length of 70 mm, controlled by the computer for setting scanning speeds and patterns. A mechanical shutter was used to switch the laser beam. A CCD camera was used to align the sample with a live view of the laser processing. The sample target was placed in open air without any pre-treatment. The setting of various parameters, the changing of the laser operating conditions, and the controlling of the scanner were all controlled using a computer.

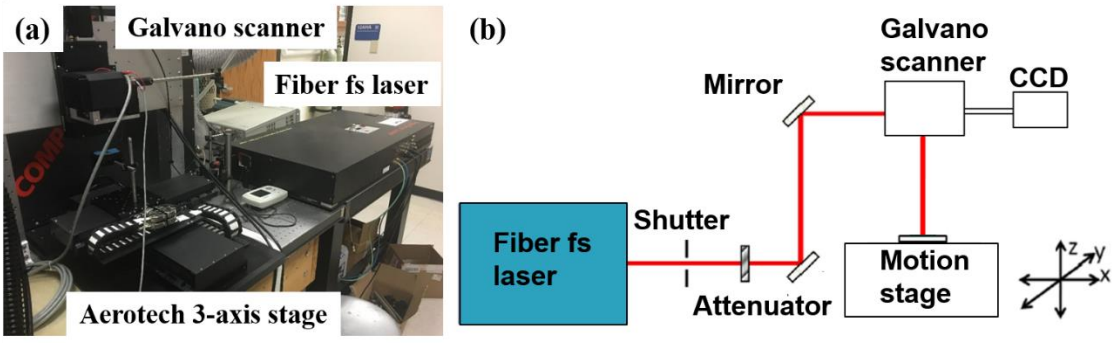

Figure 3.14: (a) A photo, and (b) a schematic illustration of the fiber fs laser drilling experiment setup.

3.4.2 Drilling Strategy

In this study, helical drilling was used. The sample was scanned with pre-determined circular pattern multiple rounds until the substrate was drilled through. The scanning path consisted of multiple circle partial filling pattern with specific pitch (distance) between the circles (see Fig. 3.15).

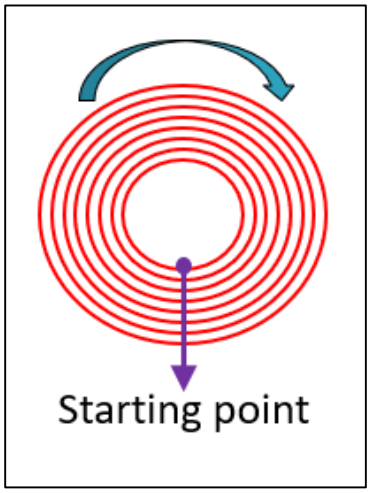

Figure 3.15: Schematic illustration of the laser scanning path.

A 2D galvanometer scanner was used to scan the laser beam on the sample. The galvanometer system moved a stationary laser beam using moving mirrors by making small adjustments in mirror angles to move the stationary laser beam in different directions within a specific marking area.

3.4.3 Results and Discussion

In this study, fiber fs laser drilling of 1 mm-diameter blind holes in a 1.6 mm LTCC substrate was demonstrated using double-side drilling strategy. Furthermore, this laser drilling process was able to process twelve holes at the same time using the

galvanometer scanner. The fiber fs laser processing is more economical and efficient than that using the Ti: Sapphire laser.

3.4.3.1 Single-side Drilling

As shown in Fig. 3.16, relatively large taper angle was obtained in the holes drilled using single side drilling strategy. The laser pulse energy was set at 150 μJ with a Z-movement speed of 3.8 μm/s, a scanning speed of 1000 mm/s, a pitch of 10 μm between the circles, and a focal position 200 μm above workpiece surface.

As shown in Fig. 3.16 (a), the boundary of drilling holes on the entrance side was smooth while the boundary on the exit side had an irregular edge. This is due to the drilling debris was sputtered out during the drilling process.

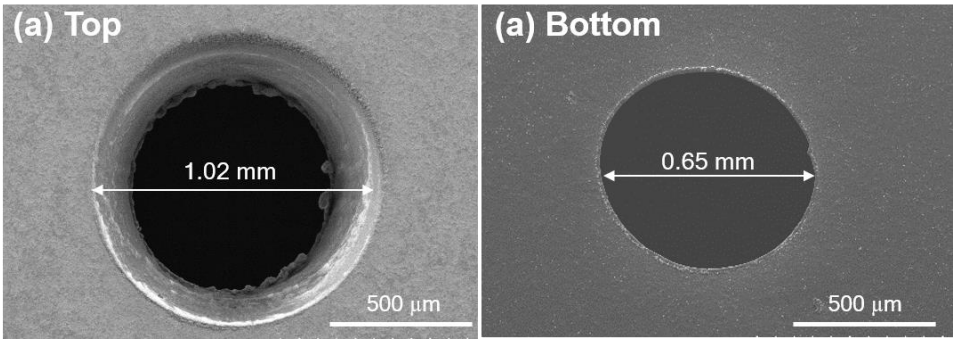

Figure 3.16: SEM images of a hole fabricated in a 1.6 mm-thick LTCC plate using single side drilling: (a) top and (b) bottom view.

As shown in Fig. 3.17, the formation of residue on the left side of the hole was observed while the right side of the hole was smooth and clean. The residue at one side of the hole was formed due to the air flow in the lab, leading to the accumulation of residue on the left side of the hole.

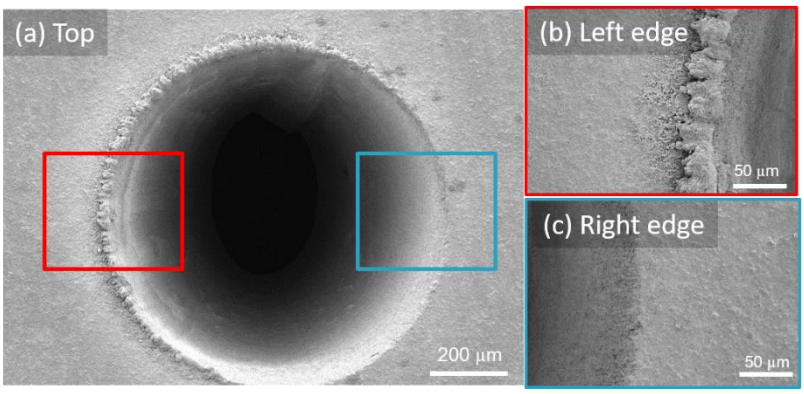

Figure 3.17: (a) SEM top image of a hole drilled using single side drilling, and high magnification images of (b) left edge, and (c) right edge.

3.4.3.2 Drilling Speed

To investigate the effect of scanning speed on taper formation, circular holes were drilled at different scanning speeds using the galvanometer scanner. The drilling was conducted at speeds from 250 to 1000 mm/s for various round numbers until the substrate was drilled through. The laser pulse energy was set at 150 µJ with a Z-movement speed of 3.8 µm/s and a pitch of 10 µm between the circles. Figure 3.18 shows the taper obtained at different scanning speeds. It was found that the drilling at higher scanning speeds produced holes with large taper, whereas drilling at a slower speed slightly reduced the hole taper.

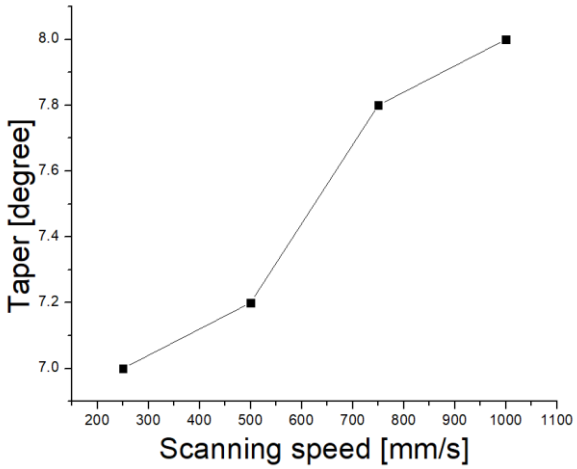

Figure 3.18: Hole taper plotted as a function of scanning speed.

This trend could be attributed to the fact that at a lower scanning speed, more pulses were delivered to a single spot and more laser pulses were overlapped during scanning of the laser beam. This resulted in higher energy delivered to one spot, and higher ablation rate during the drilling process.

3.4.3.3 Double-side Drilling

A double-side laser drilling strategy has been demonstrated to drill blind holes on LTCC substrates, with minimized taper. Laser drilling on the LTCC substrate from one side was carried out first; then the LTCC substrate was flipped and drilled from the other side at the same position to create a through-hole (see Fig. 3.19). The galvanometer scanner position accuracy was less than ±0.5 µm, enabling drilling of through-holes without displacement between the double-side drillings. The double-side drilling produced holes with minimum taper and high edge quality.

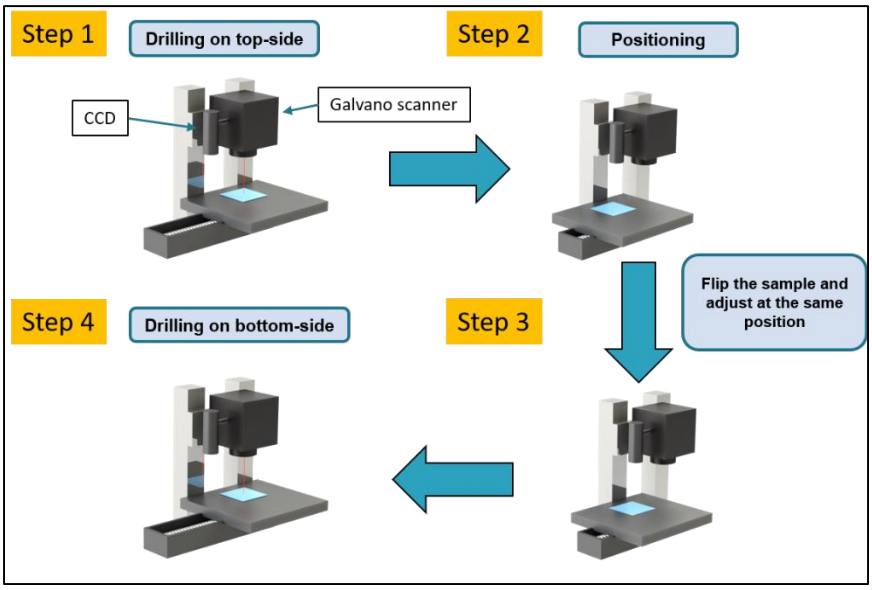

Figure 3.19: Double side drilling strategy.

For double-side drilling, a hole was first drilled from the top side. The drilling was conducted using galvanometer scanner at a scanning speed of 1000 mm/s with a pulse energy of 150 μJ, a Z-movement speed of 10 mm/s, a pitch of 75 μm between the circles, and a focal position of 200 μm above the workpiece surface. As the drill from the top side finished, the LTCC substrate was flipped and adjusted to the same position under the galvanometer scanner. Drilling using the same parameters at the same position from the back side was performed to create a through hole. Before drilling the backside hole, the CCD camera and a rotation stage were used to make sure that the center of the hole was aligned correctly with the top side hole. For the first step, the taper profile of a hole produced after the first step is shown in Fig. 3.20. The hole entrance and exit diameters were 1.02 and 0.65 mm, respectively.

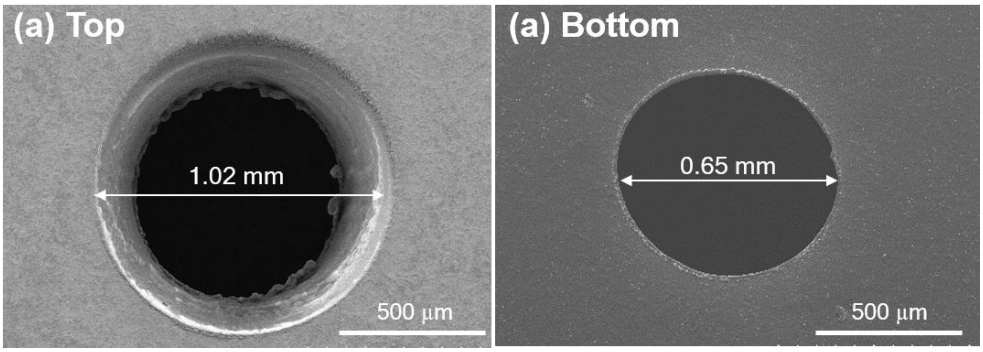

Figure 3.20: SEM images of a hole drilled after the first step during a double side drilling process: (a) top, and (b) bottom view.

In the second drilling step, a through hole was produced. As shown in Fig. 3.21 the hole entrance and exit diameters were 1.02 and 1.02 mm, respectively.

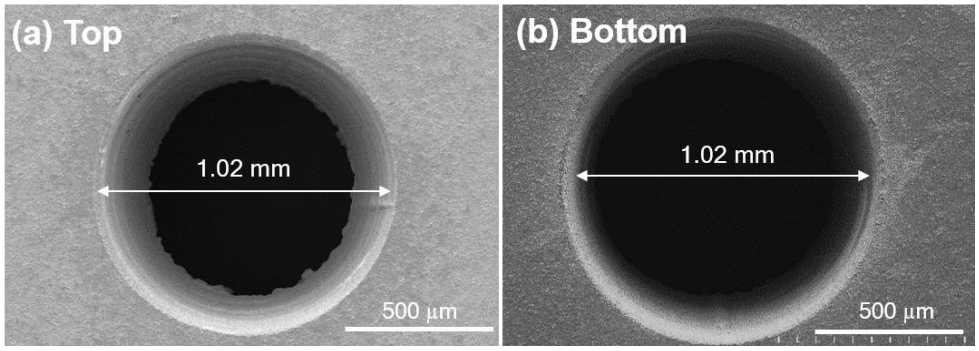

Figure 3.21: SEM images of a hole drilled after the second step during a double side drilling process: (a) top, and (b) bottom view.

With the double side drilling, a through hole with a minimum taper was drilled as shown in Fig. 3.22, with a total drilling time of 2 minutes per hole. The hole had the same entrance and exit diameters of 1.02 mm. The taper was minimized but not eliminated completely (see Fig. 3.22.b). The hole diameter at the entrance started at 1.02 mm, then decreased to 0.85 mm in the midpoint of the hole, then increased again to 1.02 mm at the exit side. The hole exit and entrance qualities were high with no debris and no HAZ observed. The thermal effects of the laser drilling were avoided due to the ultrashort pulse duration of the fs laser and the low overlap between pulses. Clearly, the taper issue was significantly reduced using double side drilling. The taper could be even further eliminated by employing higher laser power density.

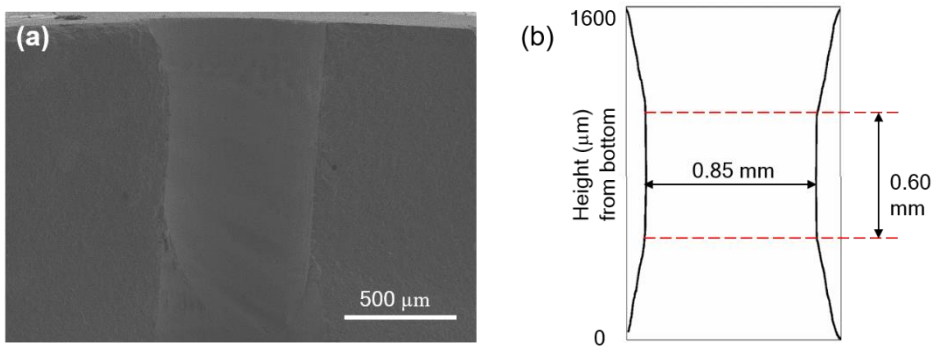

Figure 3.22: The profile of a hole drilled using double side drilling strategy: (a) a SEM cross-sectional image, and (b) a schematic illustration of the hole profile.

As shown in Fig. 3.23, LTCC drilling with clean wall surface, no visible cracks or HAZ was achieved with the optimal processing parameters.

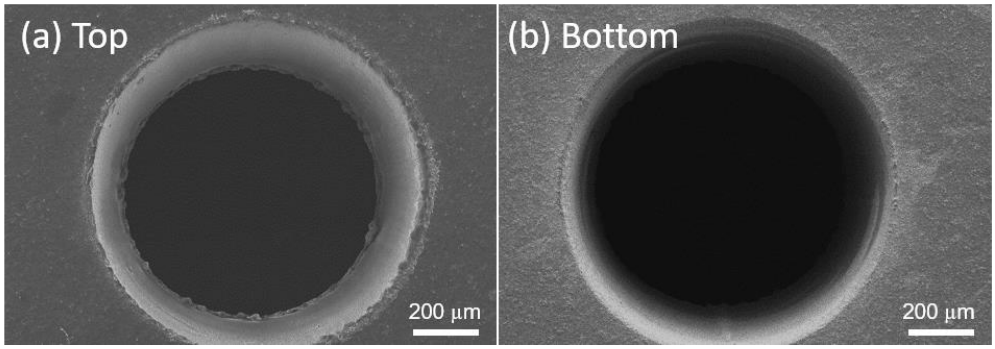

Figure 3.23: SEM images of a hole drilled using optimized parameters: (a) top, and (b) bottom view.

3.5 Summary

Femtosecond laser beam is a unique machining source. It offers high-intensity laser pulses in an exceedingly short time frame, which enables precise ablation of materials and a small HAZ. In this study, a systematic investigation on fs laser drilling of LTCC substrates was conducted. The effects of various laser processing parameters on the drilling quality of LTCC substrates in terms of HAZ, surface cleanness, cracks, recast layer and hole taper were studied. The optimal laser parameters were identified for drilling of LTCC substrates. High-quality laser drilling of LTCC substrates with a clean surface, no cracks, no recast layer and no delamination was demonstrated. Two lasers were employed to drill holes: 1) a Ti: Sapphire fs laser with a wavelength of 800 nm, and 2) a fiber fs laser with a wavelength of 1030 nm.

While both lasers showed the capability to produce high-quality holes, laser drilling with a fiber fs laser is more economical and efficient than that with a Ti: Sapphire laser with significantly reduced manufacturing time (Ti: Sapphire laser: 37 min/hole,

fiber laser: 2 min/hole). Debris-free straight holes with good roundness, clean trench edges, and no thermal damage were obtained. The developed laser drilling process of LTCC has potential applications in electronic devices.

Chapter 4: Femtosecond Laser Drilling of Glass Fiber Reinforced Polymer Printed Circuit Boards

---

4.1 Introduction

Printed circuit boards are used in most electrical and electronic equipment. They are considered to be the base of the electronics industry. The challenge of laser drilling and cutting of PCBs is related to its material composition. Typical composition would be an insulating layer of glass epoxy resin sandwiched between two copper conductive layers. Since the two materials have very different properties, refined process control is required to drill holes in PCBs at high speed and with high quality. In this study, fs laser drilling of GFRP PCB substrates was reported. The effects of various laser parameters on the laser-drilled hole quality were studied. The samples used in this study were made of GFRP PCBs material. They were 1.4 mm thick GFRP clad on both sides with 50 µm copper foil (see Fig. 4.1).

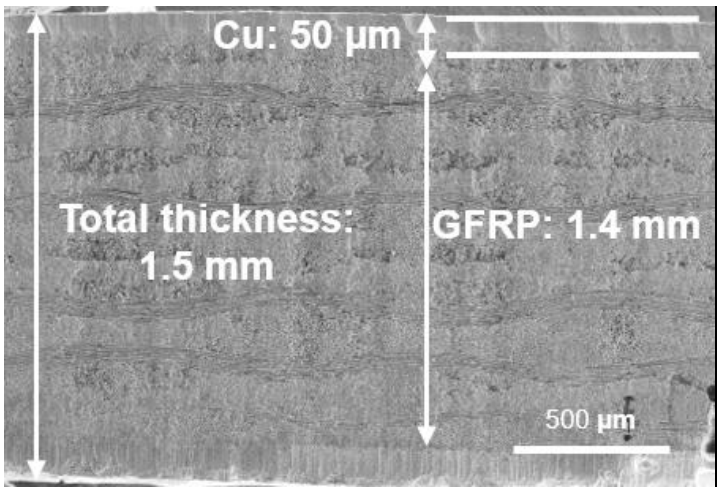

Figure 4.1: SEM cross-sectional image of a PCBs.

4.2 Material Properties

Printed circuit boards function to mechanically support and electrically connect electronic components using conductive tracks, pads and other features etched from copper sheets laminated onto a non-conductive substrate. [40] Individual electronic components (semiconductor, diodes, transistors, capacitors, resistors, inductors or active devices) are placed on the surface of the substrate and soldered to the interconnecting circuits. The base materials of PCBs are comprised of three components: the resin system, the reinforcement, and the conductive foil.

4.3 Experimental Setup

Figure 4.2 shows the schematic of the setup used for the experiment. The helical drilling source was a Ti: Sapphire fs laser system equipped with an amplifier (Legend F, Coherent Inc., 150 fs, 1 kHz, 800 μJ, and 800 nm). An attenuator was used to tune the incident laser energy. The laser beam was focused to a spot of 10 μm in diameter using a 5× objective lens (a focal length of 35 mm).

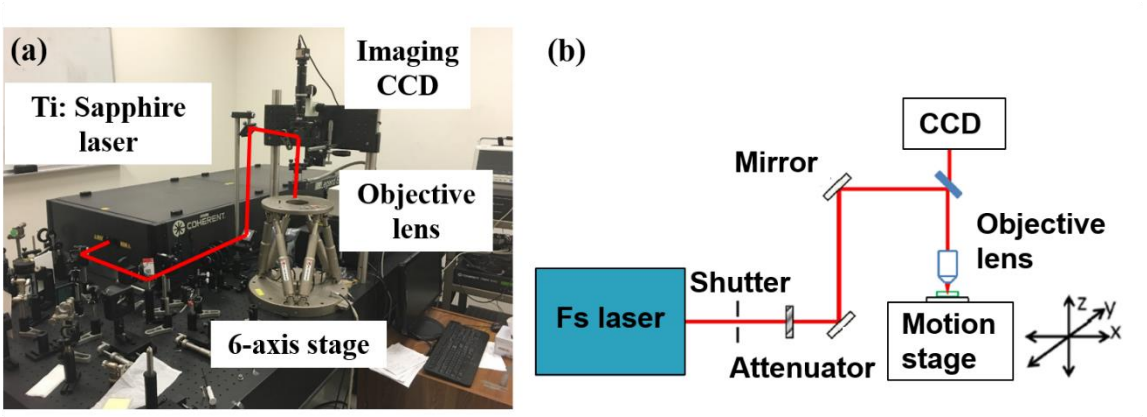

Figure 4.2: (a) A photo, and (b) a schematic illustration of the Ti: Sapphire laser drilling experiment setup.

The objective lens was enclosed in a gas flow chamber, with nitrogen (N_2) used as the assistant gas (see Fig. 4.3). The output collimated beam was a nearly symmetric Gaussian with $M_2 < 1.3$, and the maximum output pulse energy was 1 mJ. Samples were placed on a linear motion XYZ stage. The stage had a travel range of 100 mm in the X-Y direction and 50 mm in the Z direction. The maximum moving speed of the stage was 5 m/s with an accuracy of ± 2 μm. The linear motion stage was controlled by computer software. A mechanical shutter was used to switch the laser beam. A CCD camera was placed along the optical axis and used to align the sample with a live view of the laser processing. The samples were placed in open air without any pre-treatment.

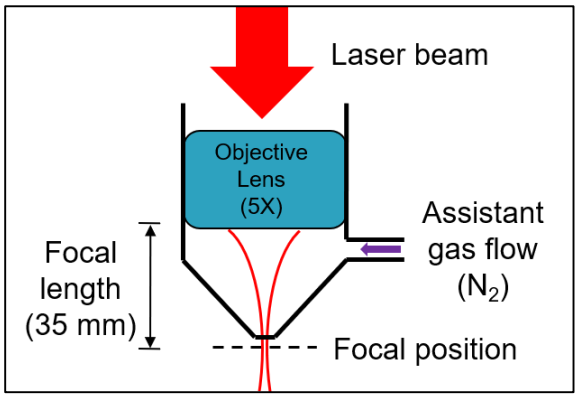

Figure 4.3: Illustration of the gas assisted focus system.

4.4 Drilling Strategy

During the drilling process, the laser beam was fixed whereas the sample was placed on a translation XYZ stage and moved in a pre-determined square path. Laser beam scanned on the sample surface along the edge of the square hole for multiple rounds until the PCB was drilled through (see Fig. 4.4).

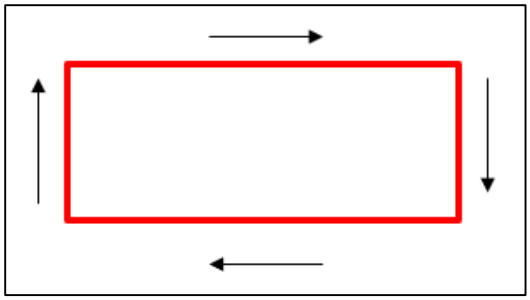

Figure 4.4: Illustration of the laser scanning path.

In order to maintain a fixed distance of the focused spot relative to the workpiece during the drilling process, the focal position started above the surface and moved down to the bottom surface step-by-step by “Pitch”. The focal position was moved after each loop, where “n” is the total drilling loops (see Fig 3.9).

4.5 Results and Discussion

In order to optimize the drilling process, the effects of the laser parameters, including pulse energy, scanning speed, focal position, and pitch, on the hole quality were investigated. The repetition rate, wavelength, and pulse duration were fixed and set to 1 kHz, 800 nm, and 150 fs, respectively. The rectangular holes were drilled in 1.5 mm thick PCBs.

4.5.1 Effects of Laser Pulse Energy on Ablation Depth and Kerf Width

The ablation depth and kerf width using different laser pulse energies were investigated. A single-line ablation test was performed, and the depth of the ablated material was plotted as a function of the laser pulse energy. The test was performed with a fixed scanning speed of 1 mm/s, and a focal position on the top surface. The results indicate that the ablation depth and the kerf width were influenced strongly by the laser

pulse energy. From Figs. 4.5 and 4.6, it is noticed that the ablation rate and the kerf width increased linearly with laser pulse energy.

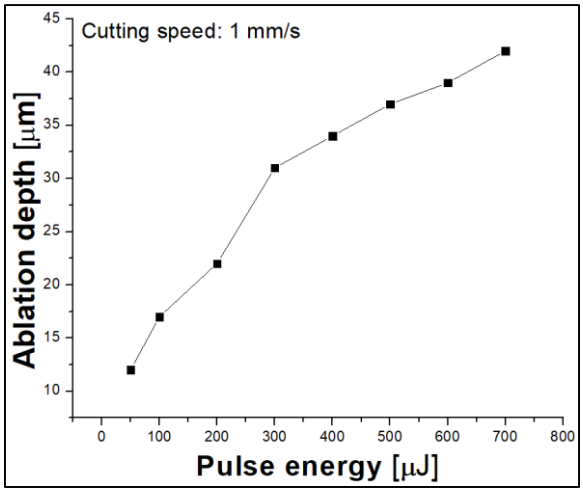

Figure 4.5: Ablation depth plotted as a function of the pulse energy at a fixed cutting speed of 1 mm/s.

The maximum depth that was drilled with a single laser scan with a pulse energy of 700 µJ was 42 µm, and the maximum kerf was 96 µm obtained at 700 µJ. In order to maximize the drilling process efficiency, laser pulse energy of 700 µJ was used to drill the PCBs material.

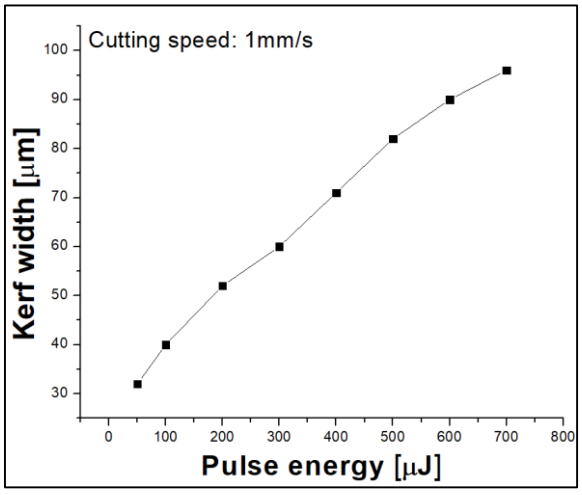

Figure 4.6: Kerf width plotted as a function of the pulse energy at a fixed cutting speed of 1 mm/s.

4.5.2 Effects of Scanning Speed

In order to investigate the impact of scanning speed on the drilling quality, single line cuts at different scanning speeds were performed. The cutting was conducted at scanning speeds from 1 to 2.5 mm/s with a laser pulse energy of 700 µJ, a focal position on top of the sample surface, and a pitch of 40 µm. Figure 4.7 shows holes drilled at different scanning speeds.

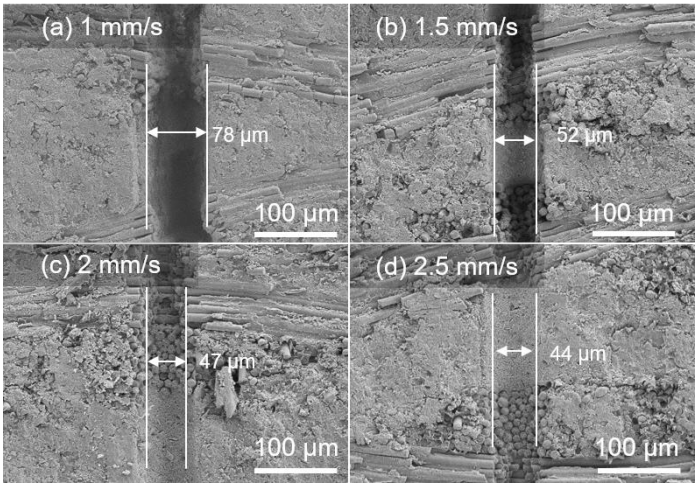

Figure 4.7: SEM top images of holes drilled in PCBs with laser pulse energy of 700 µJ at different scanning speeds: (a) 1, (b) 1.5, (c) 2, and (d) 2.5 mm/s.

Cutting at a slower speed led to a higher ablation rate, whereas cutting at a higher speed of 2.5 mm/s led to a lower ablation rate (see Fig. 4.8). Meanwhile, slower scanning speeds led to larger kerf width compared to higher scanning speeds. This trend could be attributed to the fact that at low scanning speed, more pulses were delivered to a single spot. This resulted in higher energy delivered to one spot, and higher ablation rate.

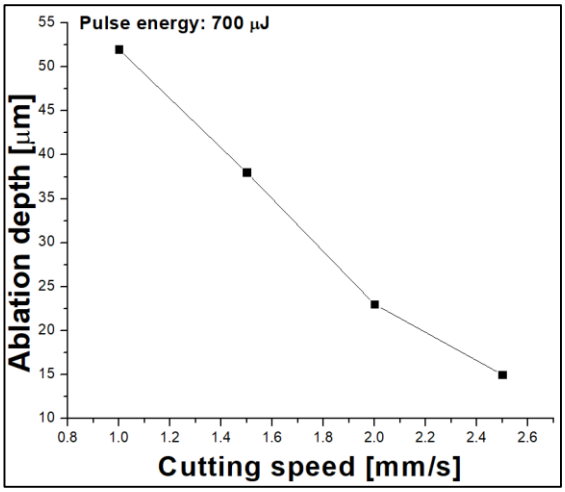

Figure 4.8: Ablation depth plotted as a function of the scanning speed at a fixed laser pulse energy of 700 μJ.

To investigate the effects of the scanning speed on the final quality, rectangular holes were drilled at different scanning speeds. The drilling was conducted at scanning speeds from 0.5 to 2 mm/s for various round numbers until the PCB substrate was drilled through. Laser pulse energy was set at 700 μJ with a focal position on top of the sample surface, and a pitch of 40 μm. Figure 4.9 shows laser-drilled holes at different scanning speeds. Slow cutting speeds led to the cavity on the sidewall. Fast speeds led to large roughness. This trend could be attributed to the fact that decreasing the scanning speed led to higher energy delivered to one spot, which in return increased the surface temperature. At higher scanning speeds, less energy was delivered to the surface on one spot, leading to the rough sidewalls. Balancing quality and efficiency, a scanning speed of 1.5 mm/s was selected as the optimal cutting speed for cutting 1.5 mm thick PCBs substrates.

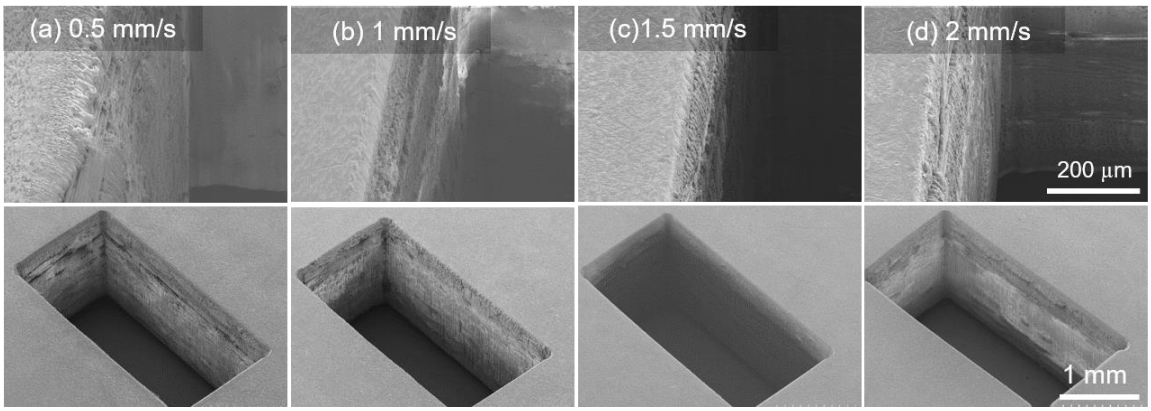

Figure 4.9: SEM images of holes drilled at 700 µJ pulse energy with different laser scanning speeds: (a) 0.5, (b) 1, (c) 1.5, and (d) 2 mm/s.

4.5.3 Effects of Focal Position

The focal position of the laser beam, at which the intensity is the highest and the beam diameter is the lowest, affected the drilling quality and taper formation significantly. The optimization process for the focal position was conducted at laser pulse energy of 700 µJ, a scanning speed of 1 mm/s, and a pitch of 50 µm. Holes were drilled at different focal positions. Figure 3.6 describes the focal position relative to the workpiece surface. A focal position of "0" is corresponded to the sample surface, a positive value (+) is for a focal position below the surface, and a negative value (−) is for a focal position above the surface. SEM cross-sectional images of holes drilled with different focal positions at a laser pulse energy of 700 µJ, a scanning speed of 1 mm/s, and a pitch of 50 µm are shown in Fig. 4.10. For holes drilled with focal positions of +400 and +200 µm, processing defects, such as wall damage and forming of debris, were observed. For drilling with focal positions of 0 and -200 µm, holes with better sidewall quality were obtained (see Fig. 4.10). The optimal sidewall quality was obtained with a focal position of -200 µm. Clean walls with no HAZ and no taper with sharp edges were observed.

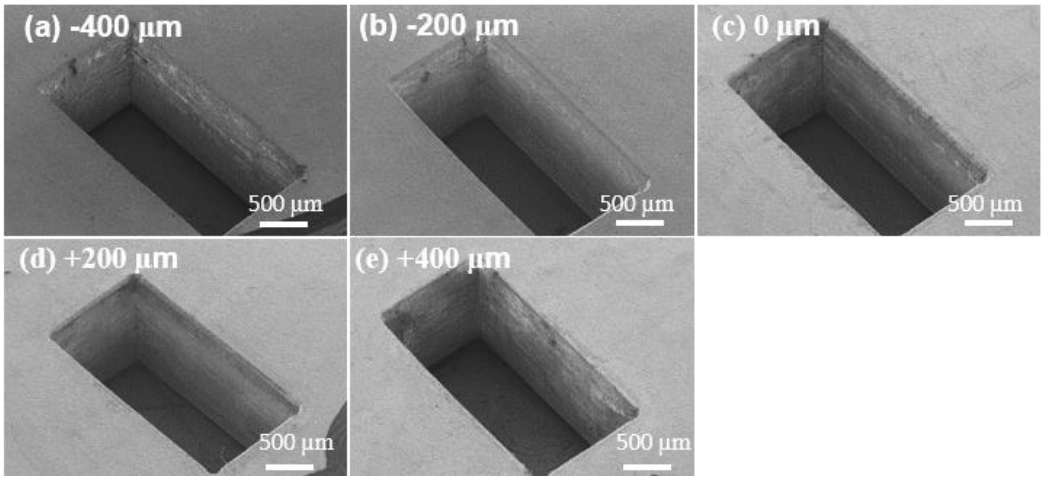

Figure 4.10: SEM cross-sectional images of holes drilled at laser pulse energy of 700 µJ with different focal positions relative to the workpiece surface: (a) -400, (b) -200, (c) 0, (d) 200, and (e) 400 µm.

Figure 4.11 shows a top surface view of the holes drilled with different laser focal positions. The results show that the focal position had less effect on top surface quality. Meanwhile, the variation in taper profile with the focal point position shows that there was an optimal focal point position, which produced a minimum taper (see Fig. 4.12).

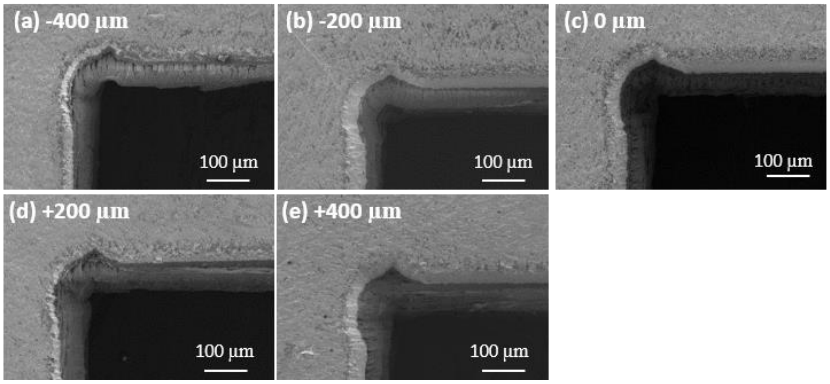

Figure 4.11: SEM images of a top view of holes drilled at laser pulse energy of 700 µJ with different focal positions relative to the workpiece surface: (a) -400, (b) -200, (c) 0, (d) 200, and (e) 400 µm.

Drilling with laser-focused above the PCBs surface led to smaller hole taper values: 3.3 ^{o} at a focal point position of -200 µm, and 3.6^{o} at -400 µm, respectively. On

the other hand, the taper increased as the focal point position moved below the surface, 5.2° at a focal point of +200 µm, and 5.8° at +400 µm, respectively. The optimal focal point position that produced the smallest taper profile for the drilling of the 1.5 mm PCBs was 200 µm above the workpiece top surface (see Fig. 4.12 (c))

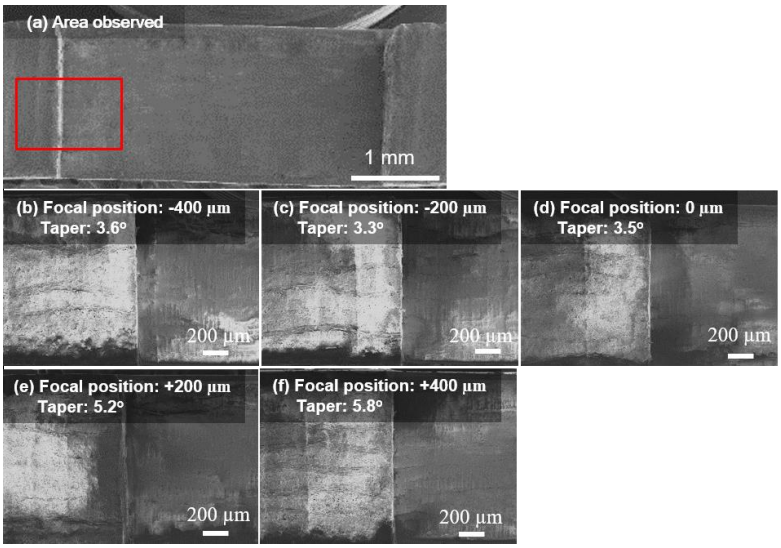

Figure 4.12: SEM cross-sectional images of holes drilled at laser pulse energy of 700 µJ with different focal positions relative to the workpiece surface: (a) area observed, (b) -400, (c) -200, (d) 0, (e) 200, and (f) 400 µm.

4.5.4 Effects of Pitch

Precisely adjusting and maintaining the distance between the sample with the laser focal position plays a key role in the drilling process. In our experiment, we found that the optimized starting location was with the laser focused 200 µm above the workpiece surface. To maintain a fixed distance of the focused spot relative to the workpiece during the drilling process, the focal position started above the surface, and then moved down to the bottom surface step-by-step by "Pitch." The focal position was moved after each scanning loop, where "n" is the total drilling loops (see Fig 3.9). To find the optimal pitch for the drilling process, rectangular holes were drilled at different

pitches. The drilling was conducted with pitch steps between 15 and 40 µm. Scanning speed was set at 1.5 mm/s, with pulse energy of 700 µJ, and a focal position 200 µm above the sample top surface, the total scanning loops was adjusted according to the pitch step. For example, a small pitch of 15 µm required 100 scanning loops for a cut through, while a larger pitch of 40 µm only required 38 scanning loops. Figure 4.13 shows the effect of the pitch on the sidewall quality. The charred material, matrix recession, and fiber protrusion were found at the hole sidewall when drilled with small pitch steps of 15 µm (see Fig. 4.13 (b)). Whereas, neither charred material nor matrix recession and cavities were observed at the hole sidewall with large pitch steps of 40 µm (see Fig. 4.13 (g)). When drilling with small pitch steps, a larger number of scanning loops was required to achieve a cut through of the material, which increased the heat accumulation on the material surface and subsequently led to HAZ, charred material, and cavities. Drilling with a larger pitch, a smaller number of scanning loops was required for a cut through, which minimized the heat accumulation on the sidewall.

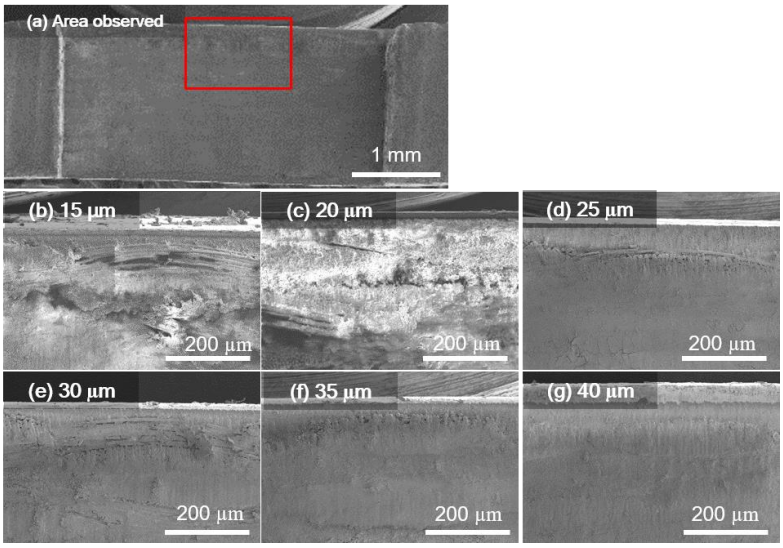

Figure 4.13: SEM cross-sectional images of holes drilled at laser pulse energy of 700 µJ with different pitch steps: (a) area observed, (b) 15, (c) 20, (d) 25, (e) 30, (f) 35, and (g) 40 µm.

The taper profile of the holes drilled with different pitches is shown in Fig. 4.14.

The diameter of the hole entrance was independent of the pitch value while the diameter of the hole exit decreased as the pitch increased, leading to a larger hole taper.

With a pitch of 25 µm, the hole profile was almost straight with no matrix recession and fiber protrusion. The pitch affected the amount of laser power delivered to the bottom surface, and the optimal pitch maximized the amount of laser power delivered to the bottom of the hole, which minimized the hole taper, and maintained high ablation rate during the drilling process by keeping the laser focused on the workpiece.

Optimal hole quality was produced with a pitch of 25 µm after each scanning loop, and a total of 60 scanning loop was required to achieve a clean cut (see Fig. 4.14 (d)).

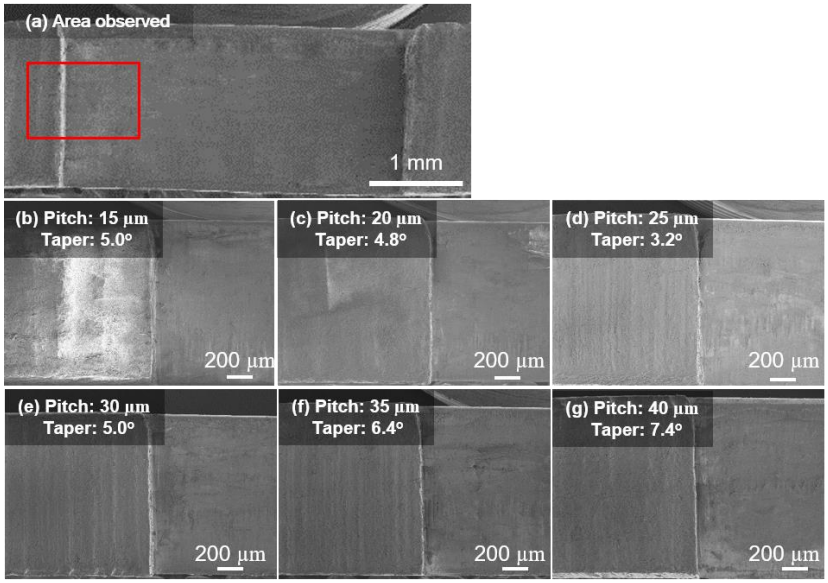

Figure 4.14: SEM cross-sectional images of holes drilled at 700 µJ pulse energy with different pitch steps and the effect of the pitch on the taper: (a) area observed, (b) 15, (c) 20, (d) 25, (e) 30, (f) 35, and (g) 40 µm.

4.5.5 Optimized Results

SEM view of the top and bottom sides of the hole drilled in a 1.5 mm thick GFRP PCB substrate in open air are shown in Fig. 4.15. The hole was drilled using the optimized parameters: a laser pulse energy of 700 µJ, a focal position of 200 µm above the sample top surface, a pitch of 25 µm, and a scanning speed of 1500 µm/s.

The hole drilled using the optimized parameters shows high-quality cutting with clean sidewall surface, no visible cracks or HAZ. The thermal effects were avoided due to the laser ultrashort pulse duration and the assist gas.

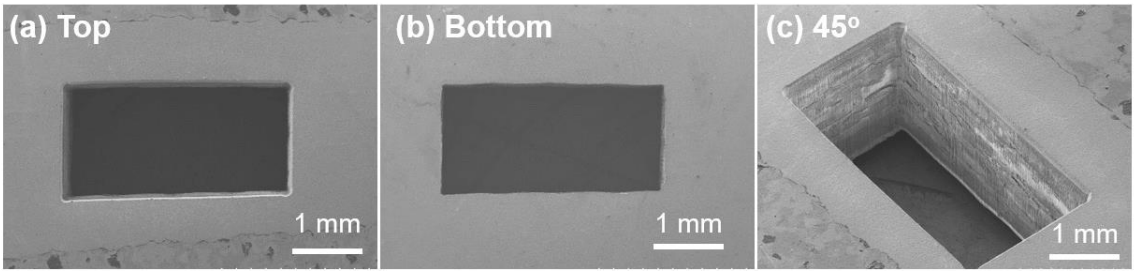

Figure 4.15: SEM images of a hole drilled using optimized parameters: (a) top, (b) bottom, and (c) 45° view.

The cross-section cuts are shown in Fig. 4.16 exhibit a very high sidewall quality: no delamination between layers, no measurable recast or HAZ, and no dross on either the surface or the edge of the hole.

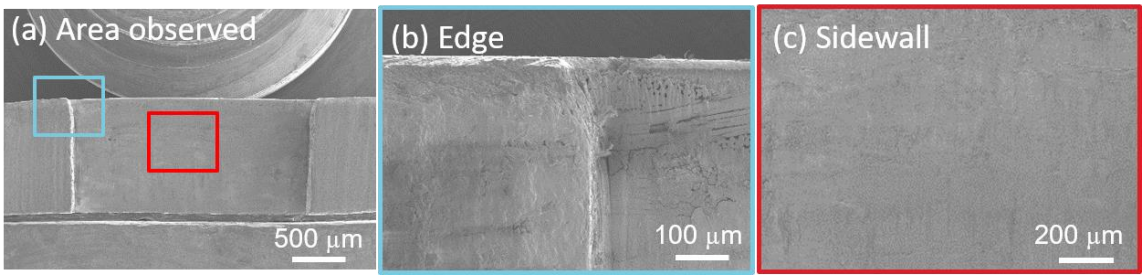

Figure 4.16: (a) SEM cross-sectional image of a hole drilled using optimized parameters, and high magnification images of (b) the drill edge and (c) hole sidewall.

4.6 Summary

In this study, fs laser drilling of GFRP PCBs has been demonstrated. The work aimed to achieve high-quality laser drilling of PCBs with minimal HAZ, clean surface finish, no debris, no recast layer, and no cracks. The effects of various laser processing parameters on the drilling quality of PCBs in terms of HAZ, surface cleanness, cracks, recast layer and hole taper were studied. The optimal processing parameters were identified for drilling PCBs substrates. High-quality laser drilling of PCBs substrates with a clean surface, no cracks, no recast layer and no delamination was demonstrated.

Chapter 5: Laser Polishing of Low-Temperature Co-Fired Ceramic

---

5.1 Introduction

Laser polishing of LTCC was performed using two lasers: excimer laser (248 nm wavelength, and 25 ns pulse duration), and fiber laser (1064 nm wavelength, and continuous wave). The experiment was conducted on an LTCC substrate with a total thickness of 1.6 mm. The samples had a characteristic micro-hillock type surface morphology with root mean square (RMS) roughness of 1.097 µm. Following the laser irradiation, the RMS value was reduced to 0.355 µm. The effects of different laser parameters on the surface roughness were evaluated.

5.2 Experiment Setup

Figure 5.1 shows the schematic of the setup used for the experiment. The LTCC sample was mounted vertically on a metal holder. The laser beam was used to scan the sample surface along an area of 8 ×8 cm^2 with a fixed scanning path.

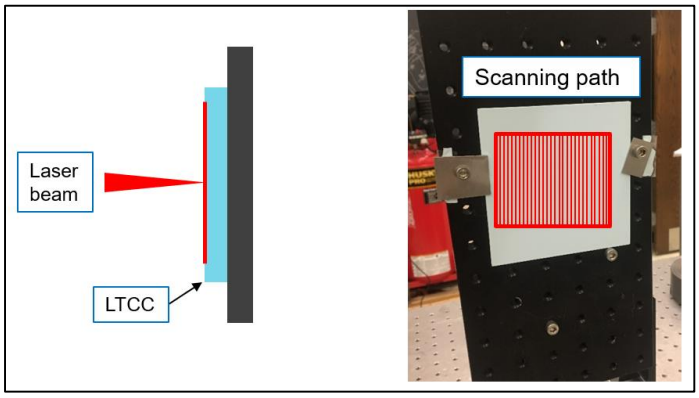

Figure 5.1: Schematic illustration of the laser polishing experiment setup.

The scanning path consisted of a square filled with vertical lines pattern with a specific pitch (distance) between lines (see Fig. 5.2).

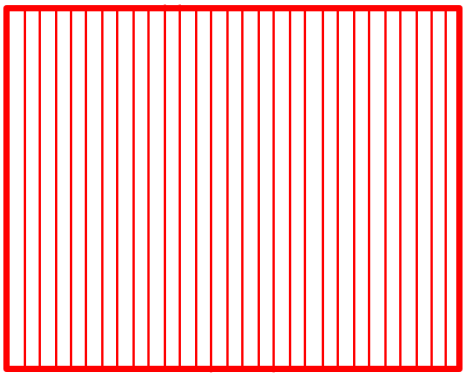

Figure 5.2: Schematic illustration of the laser scanning path.

Two lasers were employed to perform the experiment: An Excimer laser and a fiber laser. LTCC samples were irradiated by the laser beam at a normal incidence angle. The irradiation was carried out with different pulse energies, repetition rates and a number of scans. The samples were placed in the open air without any pre-treatment. A mechanical shutter was used to switch the laser beam.

5.3 Results and Discussion

Root mean square roughness of the polished LTCC was measured using a surface profiler, and the surface topography was evaluated using SEM. The effects of processing parameters, including pulse energy, pulse repetition rate, and a number of pulses, on surface roughness, were analyzed.

5.3.1 Excimer Laser Polishing

In this experiment, a 248 nm excimer laser (COMPexPro 205) with a pulse duration of 25 ns was used to polish LTCC samples using different processing parameters. The effects of processing parameters, including laser pulse energy and pulse

repetition rate, on the surface roughness were analyzed. This study aimed to investigate the efficacy of excimer laser radiation for the polishing of LTCC. Changes in surface structure due to different laser treatment were examined using SEM.

5.3.1.1 Effects of Pulse Energy

Figure 5.3 shows the effects of the pulse energy on the surface roughness of the polished LTCC samples. The surface roughness decreased as the pulse energy increased. With a laser pulse energy of 500 mJ, the polished LTCC surface consisted mainly of microcracks due to thermal stress and the rapid re-solidification as shown in Fig, 5.3 (e). Laser pulse energy between 300-400 mJ was too small to remove the LTCC material effectively. Therefore, the surface roughness of the polished LTCC was approximately the same as the original one.

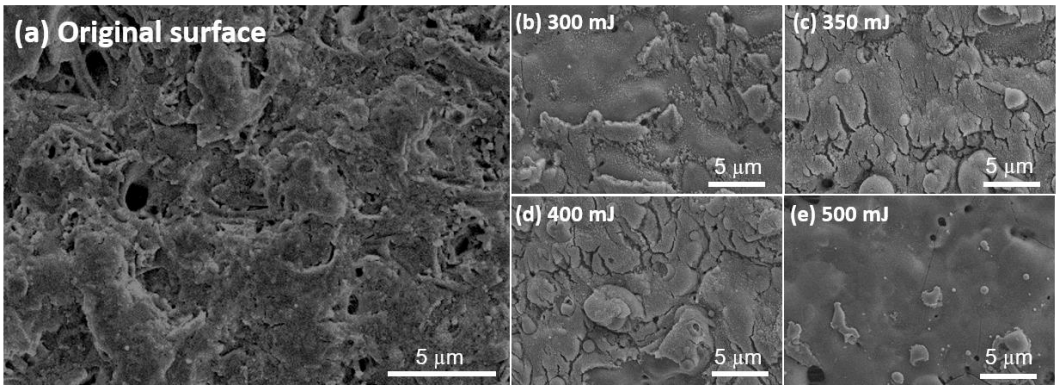

Figure 5.3: (a) SEM image of the original unpolished LTCC surface, and images of samples polished with different pulse energies: (b) 300, (c) 350, and (d) 400, and (e) 500 mJ.

5.3.1.2 Effects of Number of Laser Pulses

The surface roughness decreased as the number of laser pulses increased. However, the damage to the surrounding area also became more serious.

With laser pulses between 75-100 pulses, the smoothest surface was obtained (see Fig. 5.4). At this condition, the laser energy dissipated on the material surface increased, leading to an increase in the melting layer. As the laser pulse number decreased to 50 or lower, the laser energy became too small to remove the LTCC material effectively.

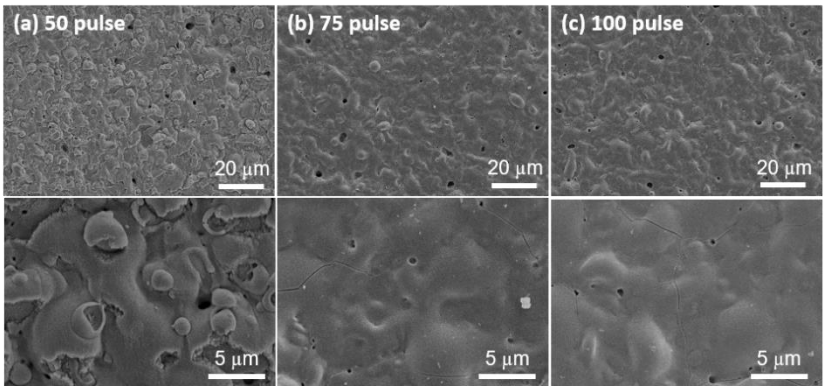

Figure 5.4: SEM images of samples polished with a different number of laser pulses: (a) 50, (b) 75, and (c) 100 pulse.

5.3.1.3 Effects of Laser Pulse Repetition Rate

The experimental results indicate that the surface roughness was influenced strongly by the laser pulse repetition rate as shown in Fig. 5.5. This is because different pulse repetition rate means different laser pulse energy. It is known that the energy per pulse equals to the average laser power divided by laser repetition rate. As laser repetition rate decreases, more energy concentrates into a single laser pulse. When the pulse repetition rate was 1 Hz, the laser pulse energy was highest, and material removal became significant comparing with processing at 5 Hz. As a result, the surface roughness decreased.

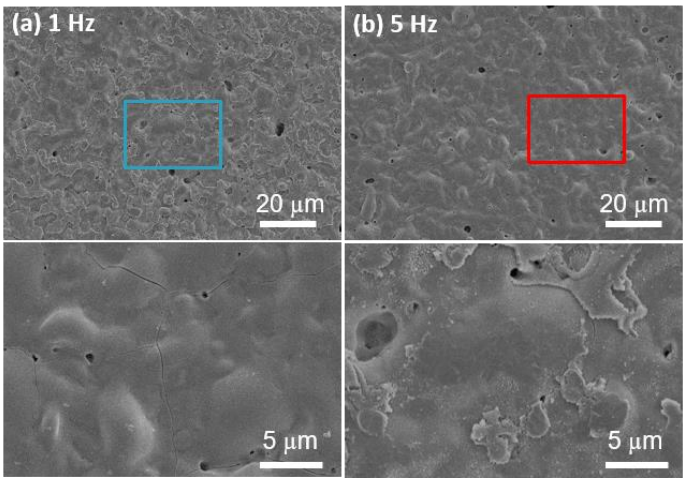

Figure 5.5: SEM images of samples polished with different repetition rates: (a) 1 and (b) 5 Hz.

5.3.2 Fiber Laser Polishing

In this study, polishing of LTCC was performed using a continuous wave fiber laser. Laser polishing of LTCC is based upon the remelting of a thin surface layer by continuous laser radiation. The laser beam heats the LTCC top surface, creating a melt pool. The laser beam was moved over the surface with a defined scanning speed, which melted the material on one side of the melt pool and re-solidified it on the other side. Due to the surface tension of the molten material, the surface roughness was smoothed during the remelting process. The resulting surface re-solidified without cracks, pores or hidden defects out of the molten material. RMS roughness of the polished LTCC was measured using a surface profiler, and the surface topography was observed using SEM.

5.3.2.1 Effects of Laser Power

In order to investigate the effects of laser power on the polishing process, LTCC samples were polished at different laser powers (see Fig. 5.6). The results indicate that the surface roughness decreased as power increased. This is due to a larger remelting depth obtained with a higher laser power. Meanwhile, with a laser power of 225 W, the

polished LTCC surface consisted mainly of microcracks due to thermal stress and the rapid re-solidification, as shown in Fig 5.6.d.

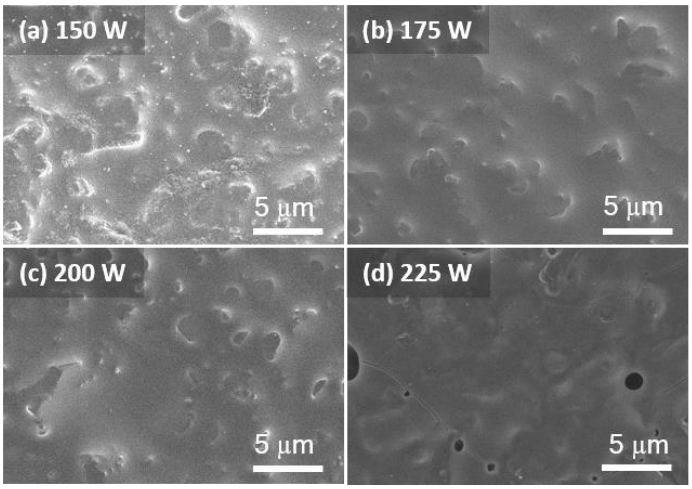

Figure 5.6: SEM images of samples polished with different laser powers: (a) 150, (b) 175, (c) 200, and (d) 225 W.

5.3.2.2 Optimize Results

As shown in Fig. 5.7, the polished LTCC sample show high-quality polishing with a clean surface, no visible microcracks, holes or debris on the surface of the substrate. The sample was polished using the following parameters: a laser power of 200 W, a scanning speed of 100 mm/s, a pitch of 0.01 mm, and five scanning loops. The polishing time was 5 minutes.

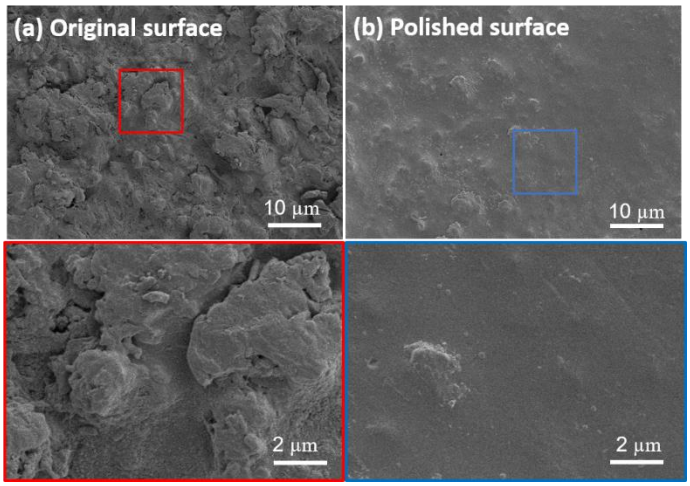

Figure 5.7: (a) SEM images of the original unpolished LTCC surface, and (b) SEM images of the polished surface using the optimized parameters.

The RMS roughness of the untreated LTCC was compared with that after the surface polishing using a surface profiler (see Fig. 5.8). The results show a significantly lower surface roughens for the polished surface compared with the untreated LTCC substrate. The RMS value of the original surface was 1.097 µm, which reduced to 0.355 µm after polishing.

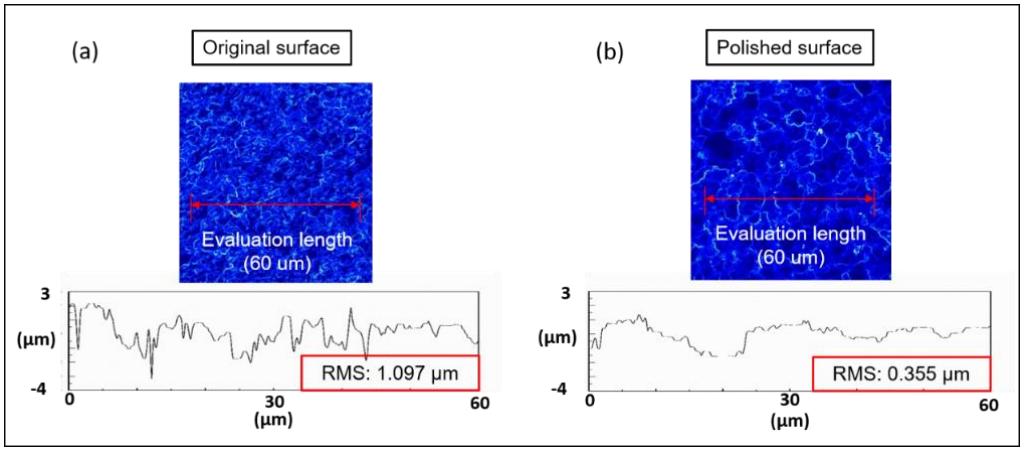

Figure 5.8: The RMS roughness of: (a) an original unpolished LTCC surface, and (b) the polished surface.

A white light interferometer system, Zygo, was used to obtain surface height data of both unpolished and polished LTCC. Figure 5.9 shows the histograms of surface heights for both samples. The results show a significant reduction in the sharp peaks slope by laser polishing, which indicates a reduction in surface roughness.

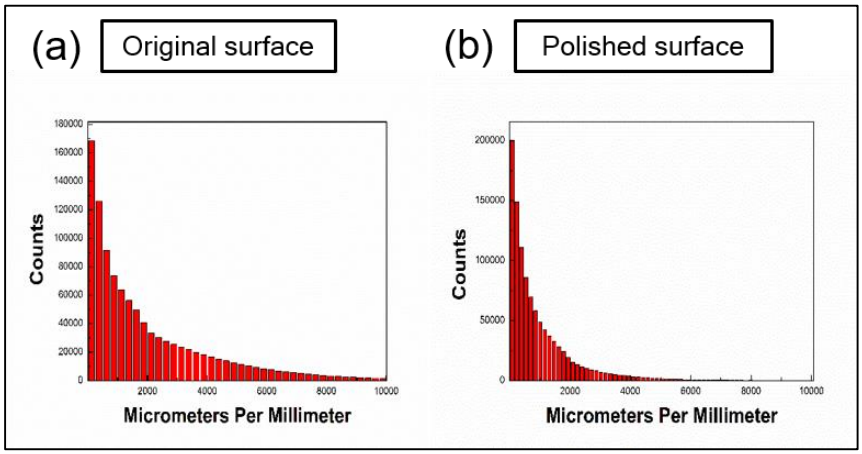

Figure 5.9: Distribution of surface heights of: (a) an original unpolished surface, and (b) the polished surface.

5.4 Summary

Two lasers were employed to polish LTCC substrates: (i) an Excimer laser (pulsed laser), and (ii) a fiber laser (continuous laser). When polishing with an excimer pulsed laser, larger surface structures remained unaffected and were not eliminated, mainly due to a small remelting depth of the pulsed laser. Continuous fiber laser was able to eliminate larger surface structures and achieve a smoother surface. The concept of laser polishing by remelting is similar to conventional polishing using fire burners, but laser provides higher control over the process since the laser beam can be controlled more precisely than a burner. RMS roughness of LTCC was reduced from 1.097 µm to 0.355

μm after polishing using a fiber continuous wave laser with a laser power 200 W, a scanning speed of 100 mm/s, a pitch of 0.01 mm, and five scanning loops.

Chapter 6: Conclusions and Recommendations for Future Work

6.1 Conclusions

6.2 Recommendations for Future Work

6.1 Conclusions

In this project, processes for fs laser drilling of LTCC and GFRP PCBs for RF packaging were developed. A high drilling quality with no trace of dross, debris and reacting layer was achieved. The effects of the laser parameters, including laser pulse energy, scanning speed, focal position, and pitch, on the hole quality, were investigated.

Femtosecond laser drilling of LTCC in open air was presented using two fs laser systems: 1) a Ti: Sapphire fs laser, and 2) a fiber fs laser. The shape and morphology of the holes were characterized and evaluated using laser microscope and SEM. After drilling, the hole taper and the HAZ were evaluated. Debris-free straight holes with good roundness, clean trench edges, and no thermal damage were demonstrated. The optimized drilling parameters were presented. Drilling of GFRP PCBs was performed using a Ti: Sapphire fs laser with N_2 as the assistant gas. The shape and morphology of the holes were characterized and evaluated using laser microscope and SEM. High-quality laser drilling with minimal HAZ, clean surface finish, no debris, no recast layer, and no cracks was achieved. The optimized drilling parameters were presented. Laser polishing of LTCC was also developed. The results showed a significant reduction in surface roughness after the laser polishing. RMS roughness of LTCC was reduced from 1.097 μm to 0.355 μm by a fiber continuous wave laser polishing. The reduction of the surface roughness is of practical importance for achieving low microwave loss since surface roughness contributes significantly to the total microwave losses.

Overall, this research demonstrated the capability of fs laser machining in the high-quality drilling of LTCC and GFRP PCBs. The effects of different laser parameters on the drilling quality were provided. This work also presented a systematic way of study

that can be followed to optimize laser machining to achieve high-quality drilling in other materials.

6.2 Recommendation for Future Work

For fiber fs laser drilling of LTCC, the taper was reduced significantly but not eliminated. Adjusting the laser beam angle of incidence during the drilling process could help to eliminate the hole taper and achieve straight walls. In order to adjust the laser beam angle during the drilling process, a 5-axis galvanometer scanner must be used. In the current study, the laser beam was kept perpendicular to the sample top surface. The Gaussian fluence profile of the laser beam resulted in wall angle (γ). The inclination of the wall leads to a larger area under the laser spot. Figure 6.1.a shows a schematic representation of the perpendicular laser beam relative to the workpiece during the drilling process.

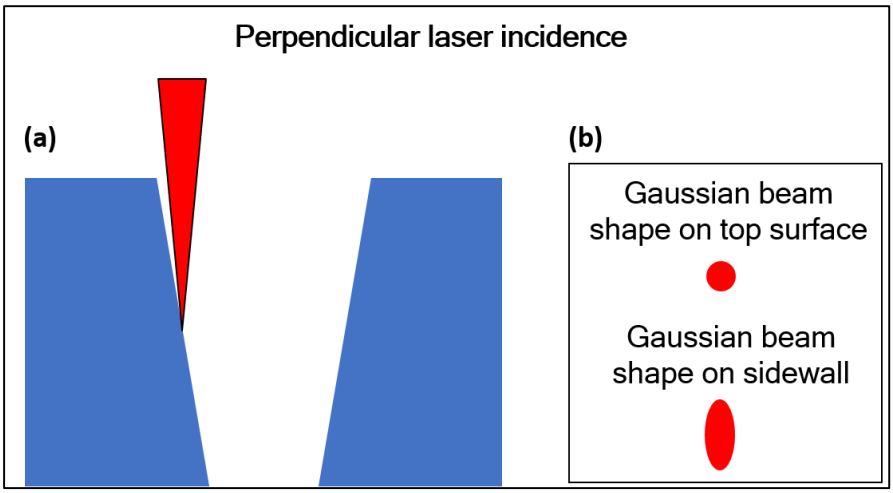

Figure 6.1: (a) Schematic illustration of perpendicular laser incidence on the workpiece and (b) laser beam profile during the drilling process.

The effective laser fluence ($\emptyset_{\text{eff}}$) on the sidewall is smaller than original laser fluence ($\emptyset_0$) by the wall angle of (γ), because the laser beam area on sidewall is much larger than original (see Fig. 6.1.b). The equation for the effective laser fluence ($\emptyset_{eff}$) is shown Eq. (2) [41]:

$$\emptyset_{\text{eff}} = \emptyset_0 \times \cos\gamma \qquad (2)$$

The larger laser spot on sidewall leads to a lower energy fluence, with lower ablation ability of the laser beam. As drilling deeper, less material could be removed, leading to the formation of a tapered hole. If drilling with the laser angle of incidence adjusted, a smaller laser area could be maintained during the drilling process, leading to higher $\emptyset_{\text{eff,}}$ than fixed perpendicular incidence (see Fig. 6.2). This makes it possible to ablate the materials on sidewall to achieve the strict perpendicular hole with the same laser pulse energy.

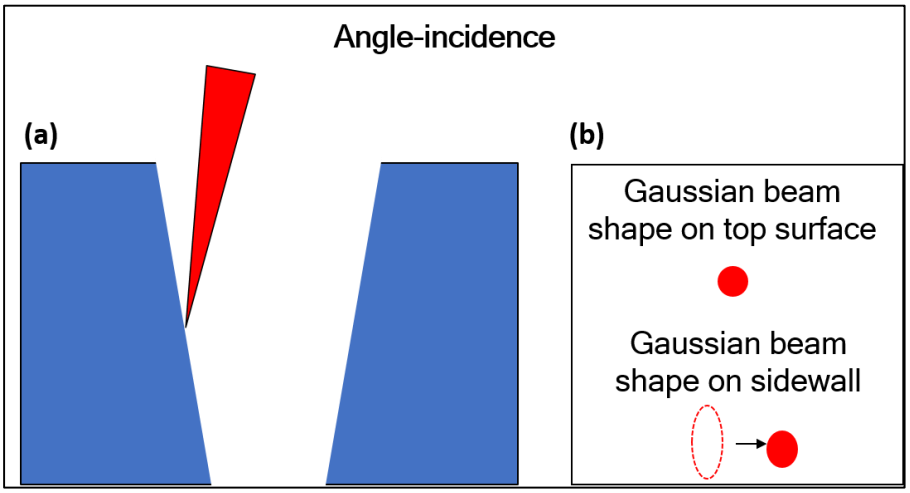

Figure 6.2: (a) Schematic illustration of angle laser incidence on the workpiece and (b) laser beam profile during the drilling process.

In the current study, the fs lasers were operated at a fixed repetition rate and a pulse duration (150 fs for Ti: Sapphire laser and 800 fs for fiber laser). The use of shorter

pulses (few fs) could achieve melting-free ablation, eliminating the recast layer formation completely. Adjusting the repetition rate to find the optimized parameter for our study could increase the ablation efficiency and reduce the drilling time. Optimizing the repletion rate could also reduce the HAZ since it controls the thermal load delivered to the sample because with a high pulse repetition rate, the time interval between successive pulses is too short for complete cooling and surface temperature increases steadily with increasing pulse number. [42] In the current study, all experiments were performed in open air, cleaner surfaces can also be expected if in vacuum conditions.

REFERENCES

[1] Silfvast, William T. “Laser fundamentals.” Cambridge university press (2004).

[2] Dahotre, Narendra B., ed. “Lasers in surface engineering.” Vol. 1. ASM international (1998).

[3] Mahamood, R. M. "Laser Basics and Laser Material Interactions." Springer (2018).

[4] Dutta Majumdar, J., and I. Manna. "Laser material processing.” International materials reviews 56.5-6 (2011).

[5] Forsman, A. C., et al. "SUPER PULSE: A NANOSECOND PULSE FORMAT FOR IMPROVING LASER DRILLING." (2007).

[6] Chen, X. "Laser drilling of advanced materials: effects of peak power, pulse format, and wavelength." Journal of laser applications, (1996).

[7] Davis, Christopher C. “Lasers and electro-optics: fundamentals and engineering.” Cambridge university press (2014).

[8] W.M. Steen, K. Watkins. “Laser Material Processing.” Springer, New York (2003).

[9] Ready, John. “Effects of high-power laser radiation.” Elsevier (2012).

[10] Dubey, A.K. and V. Yahaya. “Laser beam machining - A review.” International Journal of Machine Tools and Manufacture (2007).

[11] Parandoush, Pedram, and Altab Hossain. "A review of modeling and simulation of laser beam machining." International journal of machine tools and manufacture 85 (2014).

[12] Chua, Chee Kai, Murukeshan Vadakke Matham, and Young-Jin Kim. “Lasers in 3D Printing and Manufacturing.” (2017).

[13] Perry, M. D., et al. "Ultrashort-pulse laser machining of dielectric materials." Journal of applied physics 85.9 (1999).

[14] J.K.S. Sundar, S.V. Joshi. “Laser cutting of materials.” Centre for Laser Processing of Materials, International Advance Research Centre for Powder Metallurgy and New Materials, Hyderabad (2009).

[15] Roy, N., A. S. Kuar, and S. Mitra. "Laser Beam Micro-cutting." Non-traditional Micromachining Processes. Springer International Publishing (2017).

[16] Pham, D. T., S. S. Dimov, and P. V. Petkov. "Laser milling of ceramic components." International Journal of Machine Tools and Manufacture 47.3 (2007).

[17] Altarazi, Safwan, Leen Hijazi, and Elke Kaiser. "Process parameters optimization for multiple-inputs-multiple-outputs pulsed green laser welding via response surface methodology." Industrial Engineering and Engineering Management (IEEM), 2016 IEEE International Conference on. IEEE (2016).

[18] Zhou, Shengfeng, et al. "A comparative study of the structure and wear resistance of NiCrBSi/50 wt.% WC composite coatings by laser cladding and laser induction hybrid cladding." International Journal of Refractory Metals and Hard Materials 60 (2016).

[19] A. E. Siegman, “Lasers.” Mill Valley: Univ Science Books (1986).

[20] J.D. Majumdar, I. Manna, “Laser processing of materials.”, Sadhana 495–562, (2003).

[21] Chryssolouris, E. L. K. E, “Laser machining: theory and practice.”, Springer Science & Business Media, (2013).

[22] Dausinger, F., H. Hügel, and Vitali Konov. "Micro-machining with ultra-short laser pulses, from basic understanding to technical application." Proc. of SPIE Vol. Vol. 5147, (2003).

[23] Kannatey-Asibu Jr, Elijah. “Principles of laser materials processing.” Vol. 4. John Wiley & Sons, (2009).

[24] Dhar, Sushant, Nishant Saini, and R. Purohit. "A review on laser drilling and its techniques." Proceedings of the International Conference of Advances in Mechanical Engineering (AME 2006), Baba Banda Singh Bahadur Engineering College, Fatehgarh Sahib, Punjab, India, (2006).

[25] Soni, Alok, and R. K. Patel. "Two dimensional finite element modeling of single pulse laser drilling." International Journal of Engineering Science and Innovative Technology (IJESIT) 2.3 (2013): 389-396.

[26] Harilal, Sivanandan S., et al. "Femtosecond laser ablation: Fundamentals and applications." Laser-Induced Breakdown Spectroscopy. Springer Berlin Heidelberg, (2014).

[27] HAUPT, OLIVER, and DIRK MÜLLER. “Shorter Pulse Widths Improve Micromachining.” COHERENT INC (2013).

[28] König, Karsten, and Andreas Ostendorf, eds. “Optically induced nanostructures: biomedical and technical applications.” Walter de Gruyter GmbH & Co KG, (2015).

[29] Mishra, Sanjay, and Vinod Yadava. "Laser beam micromachining (LBMM)–a review." Optics and lasers in engineering 73 (2015).

[30] Jiang, L., and H. L. Tsai. "Femtosecond laser ablation: challenges and opportunities." NSF Workshop on Unsolved Problems and Research Needs in Thermal Aspects of Material Removal Processes, Stillwater, OK. (2003).

[31] Gamaly, Eugene G., et al. "Ablation of solids by femtosecond lasers: Ablation mechanism and ablation thresholds for metals and dielectrics." Physics of plasmas 9.3 (2002).

[32] Hamad, Abubaker Hassan. "Effects of Different Laser Pulse Regimes (Nanosecond, Picosecond and Femtosecond) on the Ablation of Materials for Production of Nanoparticles in Liquid Solution." InTech, (2016).

[33] Harilal, Sivanandan S "Femtosecond laser ablation: Fundamentals and applications." Springer Berlin Heidelberg, (2014).

[34] Mirza, Inam, et al. "Ultrashort pulse laser ablation of dielectrics: Thresholds, mechanisms, role of breakdown." Scientific reports 6 (2016).

[35] Chattopadhyay, Kalyan K. “Introduction to nanoscience and nanotechnology. PHI Learning Pvt. Ltd., (2009).

[36] P. Flewitt,” Physical Methods for Materials Characterization: Second Addition.” IOP Series in Materials Science and Engineering, 274-394 (2003).

[37] Alford, W. Jerry, R. D. VanderNeut, and Vicent J. Zaleckas. "Laser scanning microscopy." Proceedings of the IEEE 70.6 (1982).

[38] Claeys, C. L., Winnie K. Wong-Ng, and K. M. Nair. "Low Temperature Electronics and Low-Temperature Cofired Ceramics Based Electronic Devices." Journal of the Electrochemical Society (2016).

[39] Imanaka, Yoshihiko. Multilayered low temperature co-fired ceramics (LTCC) technology. Springer Science & Business Media, (2005).

[40] Marques, André Canal, José-María Cabrera, and Célia de Fraga Malfatti. "Printed circuit boards: A review on the perspective of sustainability." Journal of environmental management 131 (2013).

[41] Auerswalda J, Rucklia A, Gschwilma T. “Taper angle adjustment in ultra-short pulse laser cutting of complex micro-mechanical contours.” (2016).

[42] Gruner, Andreas, Joerg Schille, and Udo Loeschner. "Experimental Study on Micro Hole Drilling Using Ultrashort Pulse Laser Radiation." Physics Procedia 83 (2016).